GLIA

WILEY

RESEARCH ARTICLE

The expression and function of glutamate aspartate transporters in Bergmann glia are decreased in neuronal nitric oxide synthase-knockout mice during postnatal development

Vasiliki Tellios[1,2] | Matthew J. E. Maksoud[1,2] | Wei-Yang Lu[1,2,3]

[1]Graduate Program of Neuroscience, The University of Western Ontario, London, ON, Canada

[2]Molecular Medicine Group, Robarts Research Institute, London, ON, Canada

[3]Department of Physiology and Pharmacology, The University of Western Ontario, London, ON, Canada

Correspondence
Wei-Yang Lu, Department of Physiology and Pharmacology, The University of Western Ontario, N6A 5B7, London, Canada.
Email: wlu53@uwo.ca

Abstract

Bergmann glia (BG) predominantly use glutamate/aspartate transporters (GLAST) for glutamate uptake in the cerebellum. Recently, nitric oxide (NO) treatment has been shown to upregulate GLAST function and increase glutamate uptake in vitro. We previously discovered that neuronal nitric oxide synthase knockout (nNOS$^{-/-}$) mice displayed structural and functional neuronal abnormalities in the cerebellum during development, in addition to previously reported motor deficits. Although these developmental deficits have been identified in the nNOS$^{-/-}$ cerebellum, it is unknown whether BG morphology and GLAST expression are also affected in the absence of nNOS in vivo. This study is the first to characterize BG morphology and GLAST expression during development in nNOS$^{-/-}$ mice using immunohistochemistry and western blotting across postnatal development. Results showed that BG in nNOS$^{-/-}$ mice exhibited abnormal morphology and decreased GLAST expression compared with wildtype (WT) mice across postnatal development. Treating ex vivo WT cerebellar slices with the NOS inhibitor L-NAME decreased GLAST expression while treating nNOS$^{-/-}$ slices with the slow-release NO-donor NOC-18 increased GLAST expression when compared with their respective controls. In addition, treating primary BG isolated from WT mice with the selective nNOS inhibitor 7N decreased the membrane expression of GLAST and influx of Ca^{2+}/Na$^+$, while treating nNOS$^{-/-}$ BG with SNAP increased the membrane expression of GLAST and Ca^{2+}/Na$^+$ influx. Moreover, the effects of SNAP on GLAST expression and Ca^{2+}/Na$^+$ influx in nNOS$^{-/-}$ BG were significantly reduced by a PKG inhibitor. Together, these results reveal a novel role for nNOS/NO signaling in BG development, regulated by a PKG-mediated mechanism.

KEYWORDS
Bergmann glia, cerebellum, GLAST, nitric oxide, nNOS

1 | INTRODUCTION

The cerebellum is known for its role in fine motor control and coordination, and more recently has been recognized for its role in cognition and executive function (Koziol et al., 2012; Manto et al., 2012). To execute these motor functions, Purkinje neurons (PNs) in the cerebellar cortex integrate and relay synaptic inputs from both inhibitory and excitatory neurons, sending inhibitory projections to deep cerebellar

nuclei. PNs form dense synapses with glutamatergic parallel fibers (PFs) and climbing fibers (CFs) that are closely ensheathed by fine processes belonging to Bergmann glia (BG)—specialized radial astrocytes specific to the cerebellum. Along with their more common role of uptaking and recycling glutamate from the synaptic cleft of excitatory PF- and CF-PN synapses, BG play an important role during granule cell and PN development by guiding immature granule neurons from the external granular layer (EGL) to the inner granular layer (IGL) and providing a scaffold for PN dendritic growth during development (Altman, 1972; Ango et al., 2008; Lordkipanidze & Dunaevsky, 2005; Xu et al., 2013).

These excitatory synapses, in particular the PF-PN synapse, are major sites for synaptic plasticity and are heavily regulated by nitric oxide (NO) (Contestabile, 2012; Matyash et al., 2001; Wang et al., 2014). The cerebellum is one of the few sites in the central nervous system (CNS) that abundantly expresses neuronal nitric oxide synthase (nNOS)—more so than any other region of the brain (Bredt et al., 1990; Campese et al., 2006). The localization of nNOS in the cerebellum is specific to granule cells, with some localization in stellate cells, basket cells, and to some degree BG (Ihara et al., 2006; Tiburcio-Félix et al., 2019). Available evidence shows that the presence of NO in the cerebellum is crucial for the development of fine motor control and movement memory, particularly by modulating the long-term depression (LTD) profile in PNs (Daniel et al., 1998; Wang et al., 2014). NO also contributes to a normal movement phenotype, as studies in $nNOS^{-/-}$ mice showed behavioral deficits typical of ataxia when compared with age-matched wildtype (WT) mice (Huang et al., 1993; Kriegsfeld et al., 1999; Nelson et al., 1995). More recently, our group reported that $nNOS^{-/-}$ mice exhibit PN dendritic deficits that begin early in development and persist into adulthood. Specifically, we noted that mGluR1 overexpression in the $nNOS^{-/-}$ mouse resulted in increased calcium-dependent protease activity, which lead to dendritic deficits in PNs and excitotoxicity (Tellios et al., 2020).

Within the cerebellum, nNOS activity and subsequent NO production is mainly triggered by PF stimulation, as nNOS-derived NO is produced in a calcium-dependent manner. Previous studies have noted that the concentration of NO is correlated to the intensity and frequency of PF stimulation and is a key player in generating LTP in the PF-PN synapse (Namiki et al., 2005). After PF stimulation, NO production in the PF is halted by retrograde endocannabinoid signaling, through a pathway initiated by cannabinoid-1 receptors (Brown et al., 2003; Namiki et al., 2005).

Due to its highly diffusible and transient nature, NO in the cerebellum exerts its effects mainly through the classical NO-cyclic guanylyl monophosphate (cGMP)-protein kinase G (PKG) pathway. It has been reported that in the cerebellum, glutamate concentration is correlated with an increase in NOS activity, which converts the substrate L-arginine into citrulline (Bredt & Snyder, 1989).

Considering the link between NO and glutamate, it is important to recognize that the effects of NO are not limited to neurons within the cerebellum and can affect supporting cells such as BG, which are major modulators of glutamate uptake and recycling. Specialized radial astrocytes such as BG abundantly express glutamate/aspartate transporters (GLAST/EAAT1), a notable difference compared with common

cortical astrocytes that express glutamate transporter-1 (GLT-1/EAAT2) (Perego et al., 2000). In particular, GLAST has a sixfold greater expression level relative to GLT-1, making it the predominant glutamate transporter in the cerebellum (Lehre & Danbolt, 1998; Takatsuru et al., 2006). GLAST functions as a homotrimer on the plasma membrane of BG, where it transports one molecule of glutamate, as well as L−/D− aspartate by co-transporting three Na^+ and one H^+ into the cytosol, while transporting one K^+ to the extracellular space (Bauer et al., 2012). Glutamate uptake in BG is accompanied by an influx of calcium through the sodium/calcium exchanger (NCX) and calcium-permeable α-amino-3-hydroxy-5-methyl-4-isoxazolepropionicacid (AMPA) receptors (Kirischuk et al., 1997; Lopez-Bayghen & Ortega, 2004; Metea & Newman, 2006; Rojas et al., 2007), which results in an increase in nNOS-derived NO production (Kugler & Drenckhahn, 1996). Recent studies have determined that increases in NO concentrations are proportional to increases in both nNOS expression as well as GLAST functionality of cultured cerebellar BG, measured as relative D-aspartate uptake (Balderas et al., 2014; Tiburcio-Félix et al., 2019). Despite these reports, it is still unknown whether nNOS/NO signaling directly influences GLAST expression and functionality in BG during development.

Considering the importance of nNOS/NO signaling in both the dendritic development of the cerebellar PNs (Tellios et al., 2020), and GLAST function (Balderas et al., 2014; Tiburcio-Félix et al., 2019), this study sought to examine potential differences in GLAST expression and functionality in a murine model comparing WT and $nNOS^{-/-}$ cerebella across postnatal development. Specifically, the present study aimed to delineate potential changes in BG morphology and expression across development, along with functional changes of GLAST in vitro using immunocytochemistry, western blotting, and dual calcium (Ca^{2+}) and sodium (Na^+) imaging.

2 | MATERIALS AND METHODS

2.1 | Animals

WT (C57/BL6, Stock No: 000664) and $nNOS^{-/-}$ mice (B6.129S4-Nos1^tm1Plh, Stock No: 002986) were purchased from the Jackson Laboratory. All experiments were conducted in accordance with Animal Use Protocol (#2018-106) approved by the Animal Care and Veterinary Services at the University of Western Ontario.

2.2 | Immunohistochemical preparation

Intact brains from postnatal day 3 (PD3), postnatal day 7 (PD7), 2 weeks, and 7 weeks old male mice were isolated from WT and $nNOS^{-/-}$ mice and immediately placed in 4% paraformaldehyde (PFA) for 48 h. Brains were subsequently transferred to a 30% sucrose solution for at least 48 h and then sagittally sectioned at a thickness of 80 μm using a vibratome, placed in a cryoprotectant solution, and stored in −20°C until stained. Slices were first washed with PBS, then

permeabilized using a 0.25% Triton-X solution for 5 min. Free-floating slices were then blocked with a 10% normal donkey serum (NDS) solution for 1 h and incubated with the following primary antibodies overnight in 4°C: 1:500 goat anti-calbindin (CalB) (Santa Cruz Biotechnology, Dallas, TX); 1:500 guinea pig anti-GLAST (Synaptic Systems, Goettingen, Germany). Slices were washed and then incubated with the appropriate secondary antibodies for 2 h: 1:1000 anti-goat AlexaFluor 488, or 1:500 anti-guinea pig Cy3 (Jackson Immunoresearch, Burlington, ON). After incubation with the nuclear stain DAPI, slices were mounted on cover glass using Fluoromount-G (Electron Microscopy Solutions, Hatfield, PA) and images were taken using the Olympus FV1000 confocal microscope at ×60 magnification using an oil-immersion objective.

2.3 | Primary cerebellar astrocyte cultures

WT and nNOS$^{-/-}$ pups (PD 0–4) were used for acquiring primary BG cell cultures. First, pups were decapitated, and brains were quickly removed and placed in ice-cold Leibowitz L-15 media that contained 100 mg/ml bovine serum albumin and 1x penicillin/streptomycin (P/S) antibiotics (ThermoFischer Scientific, Waltham MA). Murine cerebella were carefully dissected and then homogenized by serial pipetting, first through a 10 ml pipette, then 1 ml pipette, and finally with a 200 μl pipette. Homogenized cerebella were then filtered through a 70 μm nylon filter. The filtrate was centrifuged at 900g for 4 min at room temperature. The resulting cells were resuspended in Dulbecco's modified eagle's medium (DMEM) that contained 1× P/S and 10% fetal bovine serum (FBS) (ThermoFischer Scientific, Waltham, MA). The cells were seeded in T-75 flasks containing ∼5–7 cerebella per flask. Culture media was replaced 5 days after initial plating, and subsequently every 3 days until a confluent astrocyte monolayer was present. T-75 flasks were then placed on a shaker for 2 h at 36°C and 200 rpm to dislodge any microglial cells present. After shaking, culture media and dislodged microglia were removed, and the cerebellar astrocyte monolayer was incubated with 3 ml trypsin for 5 min. After, 7 ml of DMEM supplemented with 1x P/S and 10% FBS was used to neutralize the trypsin, and cells were centrifuged at 900 g for 4 min at room temperature and resuspended in fresh culture media. Isolated cerebellar astrocytes were plated at 5×10^4 cells/ml in various culture dishes for experiments. The resulting astrocytes were primarily BG, as 90% of astrocytes within the cerebellum are identified as being BG (Martínez-Lozada et al., 2011). Within our own primary cultures, we determined the purity of BG in both WT and nNOS$^{-/-}$ astrocytes to be 91.9 ± 1.2% and 91.8 ± 1.1%, respectively (Figure S1). Specifically, BG were identified based on culture morphology and intensity of GLAST staining.

2.4 | Immunocytochemistry

Cerebellar astrocytes were seeded on poly-D-lysine coated coverglass placed in 24-well plates. Thirty minutes after specific treatments, culture media was removed and cells were fixed using 4% PFA and washed once with 0.1 M glycine, then followed by two washes with HBSS for 10 min, each. Fixed cells were then incubated with 5 μg/ml Wheat Germ Agglutinin (WGA), conjugated to CF®555 (Biotium, San Francisco, CA) for 10 min at 37°C, then washed with HBSS. Next, cells were permeabilized using a 0.1% Triton-X solution for 5 min. Cells were blocked with 5% NDS solution for 1 h and then incubated with 1:500 guinea pig anti-GLAST overnight. Primary antibodies were washed three times with HBSS for 10 min each and then incubated with 1:500 anti-guinea pig AlexaFluor 488 (Jackson Immunoresearch, Burlington, ON) for 45 min. Secondary antibodies were washed out three times with HBSS and then incubated with DAPI for 15 min at room temperature. Cells were then washed twice with HBSS, and Fluoromount-G was applied to each coverglass and then mounted onto a glass slide for imaging. Images were taken using the Nikon Ti2-E confocal microscope at ×60 magnification using an oil-immersion objective.

2.5 | Live cell calcium and sodium imaging

For conducting calcium and sodium imaging in cultured cerebellar astrocytes, culture media was washed out and replaced with a bath solution containing (in mM): 130 NaCl, 5 KCl, 3 MgCl$_2$, 2 CaCl$_2$, 5 glucose, and 10 4-(2-hydroxyethyl)-1-piperazineethanesulfonic acid (HEPES). Rhod-4 AM (AAT Bioquest, Sunnyvale, CA) and Sodium Green™ tetraacetate (ThermoFischer Scientific, Waltham, MA) were equilibrated to room temperature for 1 h before incubation with cerebellar astrocyte cultures. Each culture well was incubated with 3 μl of the calcium fluorescence indicator rhod-4 AM and 3 μl of the sodium fluorescence indicator Sodium Green tetraacetate (Lo et al., 2006) under normal cell culture conditions for 1 h. Both fluorescent indicators were then washed out using bath solution after incubation.

Thirty minutes before fluorescent imaging, astrocyte cultures were pre-treated with the following drug preparations—WT: 50 nM 7-nitroindazole 7(N); for nNOS$^{-/-}$: 250 μM S-nitroso-N-acetylpenicillamine (SNAP); for both: 10 μM arginyl-lysyl-arginyl-alanyl-arginyl-lysyl-glutamic acid (PKG$_i$) (Maksoud et al., 2020), 1 μM 2-Amino-5,-6,7,8-tetrahydro-4-(4-methoxyphenyl)-7-(naphthalen-1-yl)-5-oxo-4H-chromene-3-carbonitrile (UCPH-101, selective EAAT1 inhibitor) (Liang et al., 2014), 1 μM SEA 0400 (NCX inhibitor) (Matsuda et al., 2001). Simultaneous Ca^{2+} and Na$^+$ imaging was then performed using the EVOS FL Auto 2 system under ×20 magnification, with images documented every 10 s. Baseline Ca^{2+} and Na$^+$ levels were recorded for at least 3 min before application of 100 μM D-aspartate to stimulate GLAST activity (Balderas et al., 2014). The ratio of calcium to sodium influx was determined in order to adjust for Na$^+$ transients associated with the Na$^+$/Ca^{2+} exchanger (Rose et al., 2020). Cellular Ca^{2+}/Na$^+$ responses for each cell were normalized to their respective average baseline level using FIJI open-source software and plotted across time using GraphPad Prism 8.

2.6 | Reverse transcription quantitative polymerase chain reaction

Total RNA was isolated from primary WT and nNOS$^{-/-}$ cerebellar astrocyte cultures using the RNeasy Mini Kit (Qiagen, Toronto, ON) as per the manufacturer's instructions. Reverse transcription of 1 µg RNA to cDNA was performed using qScript™ XLT cDNA SuperMix (QuantaBio, Beverly, MA) following the manufacturer's instructions. Next, qPCR was performed using PerfeCTa SYBR Green FastMix for iQ (QuantaBio), along with 25 ng of cDNA template, and 500 nM of forward and reverse primers for SLC1A3, exon 3 (gene encoding GLAST): forward 5′CCTTGGATTTGCCCTCCGA3′; reverse 5′CTCC CCAGGGAACGAAAAGT3′. Reverse transcription quantitative polymerase chain reaction (RT-qPCR) reactions were run in triplicate along with a no-template control using a BioRad MyiQ single-color real-time PCR detection system (BioRad, Mississauga, ON). The difference in cycle thresholds (ΔCT) between the reference gene β-actin (forward: 5′CTGTCCCTGTATGCCTCTG3′; reverse 5′ATGTCACGCACGTT TCC3′) and exon 3 of SLC1A3 were graphed using GraphPad Prism 8.

2.7 | Isolation of plasma membrane proteins

2.7.1 | Membrane protein extraction kit

Primary WT and nNOS$^{-/-}$ cerebellar astrocyte cultures were washed 3× with media and then homogenized. After homogenization, a MEM-PER™ Plus Membrane Protein Extraction Kit (ThermoFisher Scientific) was used to isolate membrane-bound proteins from the sample, as per the manufacturer's instructions. The resulting samples of membrane-bound proteins were collected and stored at −80°C prior to use for western blotting.

2.7.2 | Biotinylation

After treatments, primary WT and nNOS$^{-/-}$ cerebellar astrocyte cultures were washed 3× with PBS and then homogenized in 1 ml PBS. After homogenization, cells were centrifuged for 15 s at 13,000*g* and the remaining supernatant was removed. Cells were then incubated with EZ-Link™ Sulfo-NHS-SS-Biotin (ThermoFisher Scientific) for 30 min at room temperature, with constant agitation. Astrocytes bound with biotin were washed with PBS and centrifuged to remove the supernatant. Cells were then lysed with NP-40 lysis buffer at 4°C for 30 min under constant agitation, followed by the addition of streptavidin (Sigma-Aldrich, Oakville, ON) for 1 h at 4°C. The primary astrocytes were centrifuged at 13,000 g for 5 min and the supernatant containing the cytosolic fraction was removed and stored in −80°C. Biotinylated proteins bound to streptavidin were washed 4× with PBS, then the sample was incubated in RIPA buffer for 1 h under constant agitation. Samples were then centrifuged at 13,000*g* for 5 min and the supernatant containing the plasma membrane fraction was collected and stored at −80°C prior to use for western blotting.

2.8 | Western blotting

Cerebella were isolated from WT and nNOS$^{-/-}$ mice and stored at −80°C. Cerebellar lysates were obtained by homogenizing the cerebellar tissues using a glass homogenizer in radioimmunoprecipitation assay (RIPA) lysis buffer, supplemented with 0.1% apoprotein and 0.1% leupeptin. Once homogenized, lysates were centrifuged for 30 min at 4°C. The supernatant was collected, and protein was measured using a Bradford reagent mix (Bio-Rad, Hercules, CA). Samples were later prepared using 2× sample buffer and loaded onto 8% or 10% polyacrylamide gels for electrophoresis and run for 2 h at 100 V. Gels were then wet-transferred onto nitrocellulose membranes for 2 h at 80 V. Blots were blocked in 5% bovine serum albumin (BSA) for 1 h before incubated with the following primary antibodies overnight: 1:1000 guinea pig anti-GLAST (60 and 55 kDa). Using biotinylation and a membrane extraction kit, we verified that the 60 kDa band is representative of the GLAST protein bound to the plasma membrane (PM), while the 55 kDa band is associated with GLAST within the cytosol (Figure S2). For total protein comparisons, 1:10000 anti-glyceraldehyde-3-phosphate dehydrogenase (GAPDH, 37 kDa) (Abcam, Toronto, ON) was used as a housekeeping protein. After three washes in tris-buffered saline solution, the appropriate secondary horseradish-peroxidase antibodies (Jackson Immunoresearch, Burlington, ON) were incubated on the membranes for 1.5 h. Protein was visualized using enhanced chemiluminescence substrate (Bio-Rad, Hercules, CA) and imaged using the Bio-Rad VersaDoc system. All proteins were normalized to their respective GAPDH levels. Densitometric analyses were quantified using FIJI open source software.

2.9 | Ex vivo organotypic cerebellar slice cultures

Cerebella were isolated from 10 to 12 postnatal day 0 WT and nNOS$^{-/-}$ pups in Hank's balanced salt solution (HBSS) containing: 15 mM 4-(2-hydroxyehtyl)-1-piperazineethanesulfonic acid (HEPES), 0.5% glucose, 2% sucrose, and maintained at pH 7.3 and 315 mOsm. Isolated cerebella were sliced at a thickness of 350 µm using a tissue chopper and plated on 35 mm membrane inserts (Milipore Ltd., Etobicoke, ON). The bottom half of the insert was exposed to minimum essential medium (MEM) supplemented with 5 mg/ml glucose, 25% heat-inactivated horse serum, 25 mM HEPES, 1 mM glutamine, and 100 U/ml penicillin and streptomycin. Cultures were maintained for 7 days in vitro (DIV7). Half of the medium was refreshed every 2 days. WT slices were treated with 100 µM NOS inhibitor N(G)-Nitro-L-arginine methyl ester (L-NAME) (Santa Cruz Biotechnology, Dallas, TX), while nNOS$^{-/-}$ slices were treated with slow NO-donor, 300 µM diethylenetriamine NONOate (NOC-18) (Santa Cruz Biotechnology, Dallas, TX). The cultured cerebellar slices were then used for western blotting.

2.10 | Aspartate concentration assay

Primary cerebellar astrocytes were cultured as previously described. To perform the aspartate assay, culture medium was replaced with

serum-free culture medium for at least 2 h. Drug pretreatments (for WT: 50 nM 7N; for nNOS$^{-/-}$: 250 μM SNAP; for both: 10 μM PKG$_i$) were applied for 30 min prior to application of 100 μM L-aspartate for another 30 min. After treatment, cells were lysed and L-aspartate levels were measured using the Aspartate Assay Kit (Sigma-Aldrich, Darmstedt, Germany) and performed in accordance with the manufacturer's instructions.

2.11 | Image analysis

2.11.1 | BG lamellar process thickness quantification

BG lamellar process thickness reports the diameter of largest smooth radial processes, visualized using GLAST fluorescent staining, that are visible in the EGL, present in PD3 and PD7 WT and nNOS$^{-/-}$ mice. Briefly, the 10 largest processes were identified per image and measured in micrometers (μm) using the straight-line tool on FIJI. BG lamellar process thickness was averaged from multiple images across four biological replicates.

2.11.2 | Colocalization analysis

Immunohistochemical images stained with both GLAST and CalB were converted separately into masks using FIJI open-source software. Next, the GLAST mask was overlayed onto the CalB mask, and the image was subtracted to reveal the area of GLAST + CalB per 60x image taken. This area of overlap consisting of GLAST + CalB was then normalized to the total area of GLAST staining to obtain a percent area (% area) of GLAST colocalizing to CalB. The resulting % areas were graphed using GraphPad Prism 8.

2.11.3 | Immunocytochemistry PM/cytosol expression quantification

To determine changes in PM and cytosolic localization of GLAST across a variety of pharmacological treatments, an image analysis protocol as detailed in a previous report (Maksoud et al., 2019) was adapted for cultured BG. Briefly, WGA (staining the plasma membrane of the cells) was used to determine the outer borders of each BG in culture. The WGA stain was then thresholded and converted into a mask using FIJI. Entire cell regions of interest (ROIs) were obtained corresponding to each cell within the imaged culture well, and each ROI was further eroded to create an ROI denoting the BG cytosol (Maksoud et al., 2019). A PM mask for each cell was then made by subtracting the cytosol mask from the entire cell mask. The PM and cytosol mask of each cell was then overlayed onto the GLAST fluorescent image, and the integrated density of each region was measured to determine a PM/cytosol ratio for each cell. The PM/cytosol ratio of

GLAST fluorescence for all individual cells per treatment group were averaged and graphed using GraphPad Prism 8.

2.12 | Statistical analysis

Statistical analyses were performed using an unpaired, two-tailed t test for all results comparing WT to nNOS$^{-/-}$ mice. Results obtained from immunocytochemistry PM expression were analyzed using a one-way analysis of variance (ANOVA) corrected with a Tukey's post hoc test. Significance was determined using a threshold of $p = .05$. All values are reported as mean ± SEM.

3 | RESULTS

3.1 | nNOS regulates BG morphology and GLAST expression in the cerebella of mice during postnatal development

GLAST is highly expressed in specialized radial astrocytes and is a biomarker for cerebellar BG. Therefore, we first investigated whether the morphology of BG as well as the expression and localization of GLAST are altered during postnatal development in nNOS$^{-/-}$ cerebella by comparing to age-matched WT mice. Immunohistochemical analysis from WT and nNOS$^{-/-}$ cerebella at PD3 revealed GLAST expression within the IGL and the EGL. GLAST expressing BG processes surrounded the cell bodies and sparse dendritic processes of PNs, marked by CalB staining, and BG lamellar processes were easily visible (Figure 1a). To further examine BG morphology, we analyzed the percent of GLAST coverage to CalB staining between WT and nNOS$^{-/-}$ cerebella. Our analyses revealed more GLAST-PN coverage in WT cerebella compared with nNOS$^{-/-}$ cerebella at PD3 (Figure 1b). Additionally, nNOS$^{-/-}$ BG displayed thicker lamellar processes when compared with WT BG at PD3 (Figure 1c). Our western blot analysis for GLAST expression in cerebellar tissues revealed a significant downregulation of GLAST protein expression in nNOS$^{-/-}$ cerebella when compared with WT cerebella at PD3 (Figure 1d).

At PD7, cerebellar cortex organization was more apparent and PN dendritic processes were more visible. It is important to note that PN dendrites at this developmental time point differ significantly between WT and nNOS$^{-/-}$, as described in prior experiments from our group (Tellios et al., 2020). GLAST staining of BG extended to all layers of the cerebellar cortex in PD7 mice (Figure 2a). However, the majority of GLAST expression remained close to the cell bodies and dendrites of PNs. Image analyses showed that the percentage of GLAST-CalB overlay was significantly lower in nNOS$^{-/-}$ cerebella compared with WT cerebella at PD7 (Figure 2b). BG lamellar processes were prominent in both WT and nNOS$^{-/-}$ BG at PD7, however, significantly thicker processes were observed in nNOS$^{-/-}$ BG compared with age matched WT BG (Figure 2c). Our western blot analysis revealed significantly less GLAST expression in nNOS$^{-/-}$ cerebella compared with WT cerebella at PD7 (Figure 2d).
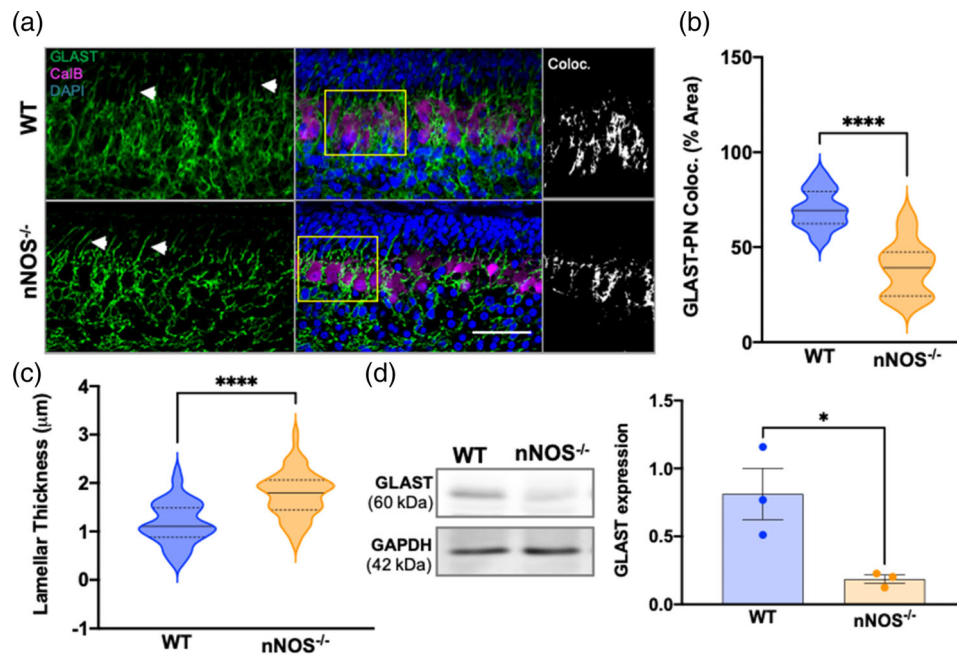
FIGURE 1 BG-PN colocalization and total GLAST expression decreased at PD3 in nNOS$^{-/-}$ cerebella compared with WT. (a) Representative confocal images of WT and nNOS$^{-/-}$ cerebella showing GLAST (green) in BG, CalB (magenta) in PNs, and nuclei stained with DAPI (blue). White arrows point to BG lamellar processes. Scale bar represents 50 μm. Depicted in the third panel are representative images of GLAST-CalB colocalization analysis, with white representing the area of GLAST+CalB overlay. (b) Violin plots represent the area of GLAST+CalB overlay in relation to total CalB staining within a consistent ROI size, presented as % area. $N = 4$ biological replicates per group; WT $n = 20$ ROIs, nNOS$^{-/-}$ $n = 12$ ROIs. $p < .0001$. (c) Violin plots represent lamellar process thickness, measured in μm. $N = 4$ biological replicates per group. WT $n = 58$ processes, nNOS$^{-/-}$ $n = 79$ processes. $p < .0001$. (d) Representative western blot of total GLAST protein expression for PD3 WT and nNOS$^{-/-}$ cerebella and the housekeeping protein GAPDH. Bar graph reports GLAST expression normalized to GAPDH. $N = 3$ biological replicates per group. $p = .0302$

At 2 weeks, the structural organization of the cerebellum is similar to the organization of the mature cerebellar cortex—the lamellar processes are functionally dissolved along with the EGL, and the IGL is now referred to as the granular cell layer. Immunohistochemical assays showed that nearly all GLAST expression was localized to the PN layer and the molecular layer, with little to no staining present in the granular cell layer (Figure 3a). Similar to earlier time points, our imaging analyses showed a significant decrease in the percent of GLAST-CalB colocalization in nNOS$^{-/-}$ cerebella compared with WT cerebella at 2 weeks (Figure 3b). At this time point, total GLAST protein expression was significantly decreased in nNOS$^{-/-}$ cerebella compared with WT cerebella, evidenced by our western blot analyses (Figure 3c).

The majority of GLAST expression in 7 weeks mice cerebella was concentrated to the PN layer and the molecular layer, with little to no GLAST immunofluorescence observed in the granular cell layer (Figure 4a). The percent of GLAST-CalB colocalization was significantly lower in nNOS$^{-/-}$ cerebella compared with age matched WT cerebella (Figure 4b). Western blotting in nNOS$^{-/-}$ cerebella at 7 weeks revealed a significant decrease in GLAST protein expression when compared with age-matched WT cerebella (Figure 4c). Together, results from our immunohistochemical and biochemical analyses showed that the absence of nNOS critically regulates BG

morphology and decreases GLAST protein expression during postnatal development.

3.2 | NO upregulates GLAST expression in organotypic cerebellar slice cultures and intracellular L-aspartate levels in cultured BG

To determine whether NO regulates the expression level of GLAST in a functional paradigm, we established ex vivo organotypic cultures of cerebellar slices from PD0 WT and nNOS$^{-/-}$ mice. After treating the WT or nNOS$^{-/-}$ cerebellar slice cultures for 7 days with pharmacological agents that would either inhibit NO production or increase NO concentration respectively, the expression of GLAST protein was assayed using western blot. Results showed that after treatment with L-NAME, the expression level of GLAST in WT cerebellar slice cultures was significantly decreased compared with control WT slice cultures (Figure 5a). On the other hand, nNOS$^{-/-}$ slices treated with slow-release NO-donor NOC-18 showed a significant increase in GLAST expression when compared with control nNOS$^{-/-}$ slice cultures (Figure 5b). These results demonstrated that NO regulates the expression level of GLAST in cerebellar astrocytes.

To examine whether endogenous nNOS/NO has any effect on L-aspartate levels within BG, we cultured primary astrocytes and mea-
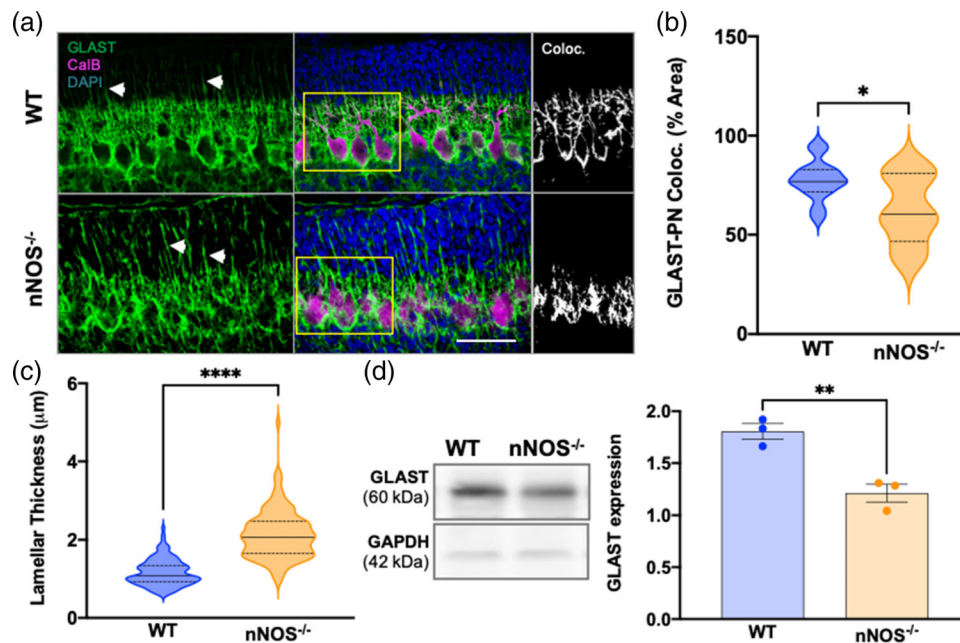
FIGURE 2 BG-PN colocalization and total GLAST expression decreased at PD7 in nNOS$^{-/-}$ cerebella compared with WT (a) representative confocal images of WT and nNOS$^{-/-}$ cerebella showing GLAST (green), CalB (magenta), and nuclei stained with DAPI (blue). White arrows highlight BG lamellar processes. Scale bar represents 50 μm. Depicted in the third panel are representative images of GLAST-CalB colocalization analysis with white representing the overlay of GLAST+CalB staining. (b) Violin plots represent the area of GLAST+CalB staining in relation to total CalB staining within a consistent ROI, represented as % area. $N = 4$ biological replicates per group; WT $n = 14$ ROIs, nNOS$^{-/-}$ $n = 8$ ROIs. $p = .0161$. (c) Violin plots represent lamellar process thickness, measured in μm. $N = 4$ biological replicates per group. WT $n = 125$ processes, nNOS$^{-/-}$ $n = 112$ processes. $p < .0001$. (d) Representative western blot of total GLAST protein expression for PD7 WT and nNOS$^{-/-}$ cerebella and housekeeping protein GAPDH. Bar graph represents GLAST protein expression normalized to GAPDH. $N = 3$ biological replicates per group. $p = .0065$

sured L-aspartate concentrations between WT and nNOS$^{-/-}$ cultures. Our assay showed that 30 min after treatment with 100 μM L-aspartate, nNOS$^{-/-}$ BG exhibited a significantly lower level of cytosolic L-aspartate compared with WT BG (Figure 5c).

3.3 | Plasma membrane GLAST expression can be modulated by NO production in vitro

Considering that NO signals mainly through the classical PKG pathway, we next investigated whether NO-PKG signaling regulates the expression and subcellular localization of GLAST in cultured WT and nNOS$^{-/-}$ BG. Specifically, WT cells were either left untreated (CON), or treated with either 50 nM 7N or with 10 μM PKG$_i$. BG were identified based on their intense staining of GLAST. WT CON BG exhibited GLAST fluorescence that was localized to the plasma membrane, as determined by localization with WGA (Figure 6a). In contrast, 7N treatment significantly decreased GLAST fluorescence on the plasma membrane and increased GLAST internalization when compared with WT CON cells (Figure 6a). Treatment of PKG$_i$ did not affect plasma membrane localization of GLAST when compared with WT CON BG (Figure 6a). Similarly, western blot assays revealed a significant decrease in GLAST protein expression in 7N treated WT BG when compared with CON WT and PKG$_i$-treated WT BG (Figure 6b).

nNOS$^{-/-}$ BG were either left untreated (CON) or treated with either 250 μM SNAP or with a combination of SNAP and PKG$_i$ (SNAP+PKG$_i$). The nNOS$^{-/-}$ CON BG had considerably less GLAST fluorescence localized near the plasma membrane in comparison to the WT CON cultures. Importantly, SNAP-treated nNOS$^{-/-}$ BG had significantly more GLAST localized on the plasma membrane than the CON nNOS$^{-/-}$ BG. Notably, nNOS$^{-/-}$ cells treated with SNAP+PKG$_i$ showed a similar amount of GLAST localization on the plasma membrane when compared with CON nNOS$^{-/-}$ BG, but significantly less plasma membrane localization of GLAST when compared with SNAP-treated nNOS$^{-/-}$ BG (Figure 7a). Western blotting of GLAST protein in nNOS$^{-/-}$ BG revealed an increase in GLAST expression within the SNAP-treated BG when compared with CON and SNAP+PKG$_i$-treated nNOS$^{-/-}$ BG (Figure 7b).

3.4 | GLAST transcription is not affected by nNOS deletion in cultured BG

To determine whether the differences in GLAST protein expression and localization can be attributed to changes in transcriptional activity of the SLC1A3 gene, we performed RT-qPCR on primary WT and nNOS$^{-/-}$ cerebellar astrocyte cultures (Figure 8). Interestingly, no significant differences in transcription of SLC1A3 were noted between
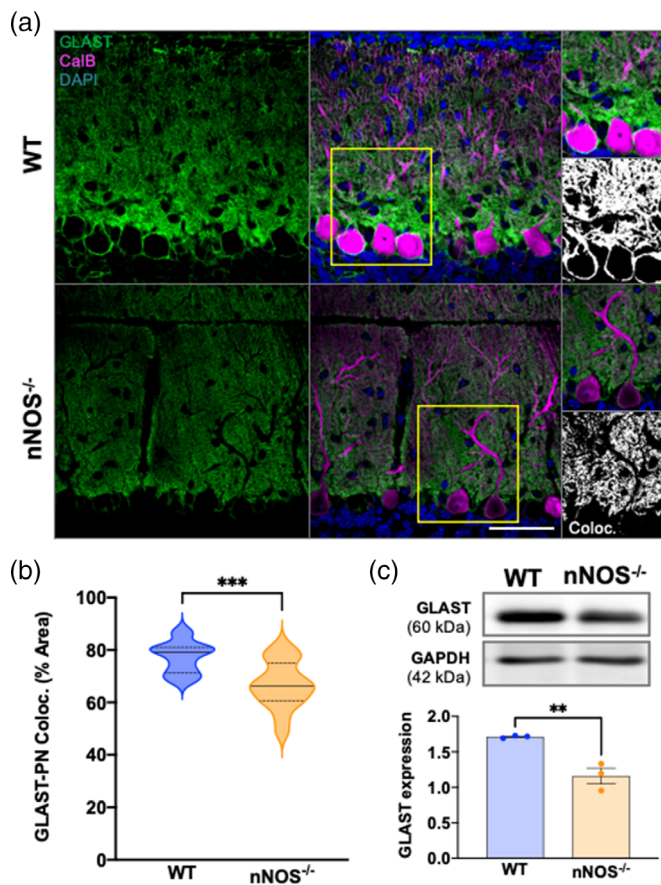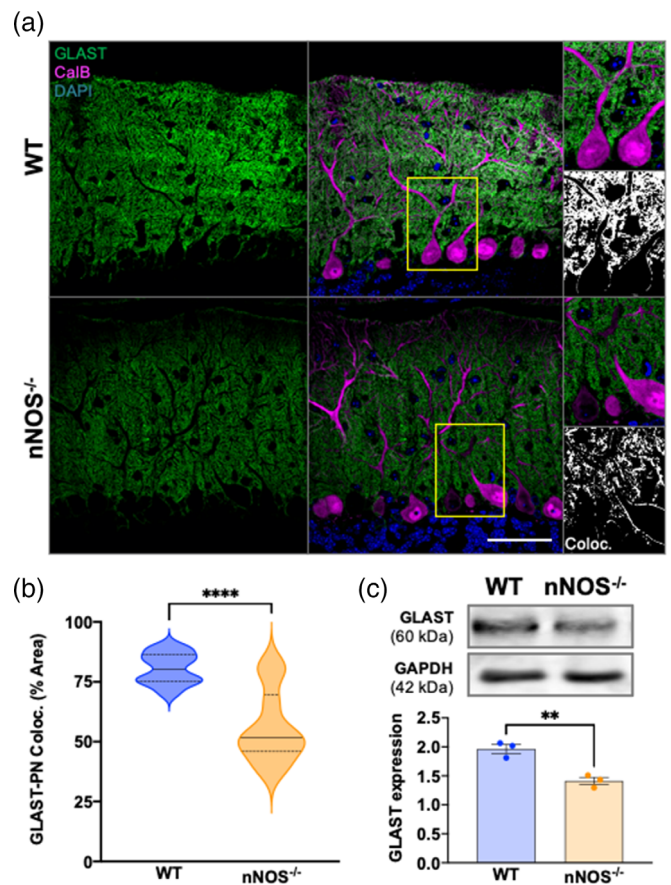
FIGURE 3 BG-PN colocalization and total GLAST expression is decreased in 2 weeks nNOS$^{-/-}$ cerebella compared with WT. (a) Representative confocal images of GLAST (green) and CalB (magenta) expression in WT and nNOS$^{-/-}$ cerebella with nuclei stained by DAPI (blue). Scale bar represents 50 μm. Representative image of GLAST-CalB colocalization analysis depicted in the third panel, with white representing the area of GLAST+CalB overlay. (b) Violin plots represent the area of GLAST+CalB overlay in relation to the total area of CalB staining within a consistent ROI, represented as % area. $N = 4$ biological replicates per group; WT $n = 14$ ROIs, nNOS$^{-/-}$ $n = 16$ ROIs. $p = .0009$. (c) Representative western blot of total GLAST protein expression in 2 weeks WT and nNOS$^{-/-}$ cerebella and housekeeping protein GAPDH, along with bar graph presenting GLAST expression normalized to GAPDH. $N = 3$ biological replicates per group. $p = .0077$

FIGURE 4 BG-PN colocalization and total GLAST expression is decreased in 7 weeks nNOS$^{-/-}$ cerebella compared with WT. (a) Representative confocal images of WT and nNOS$^{-/-}$ cerebella expressing GLAST (green) and CalB (magenta) with nuclei stained with DAPI (blue). Scale bar represents 50 μm. Representative image of GLAST-CalB colocalization analysis are depicted in the third panel, with white representing common GLAST+CalB overlay. (b) Violin plots represent the area of GLAST+CalB overlay in relation to the total area of CalB staining within a consistent ROI, represented as % area. $N = 4$ biological replicates per group; WT $n = 12$ ROIs, nNOS$^{-/-}$ $n = 10$ ROIs. $p < .0001$. (c) Representative western blot of total GLAST protein expression for 7 weeks WT and nNOS$^{-/-}$ cerebella and the housekeeping protein GAPDH, along with bar graph representing GLAST expression normalized to GAPDH. $N = 3$ biological replicates per group. $p = .0053$

WT and nNOS$^{-/-}$ BG cultures. These results indicate that increased protein expression of GLAST on the membrane is due to an alteration in GLAST protein trafficking rather than a change in transcription of the SLC1A3 gene.

3.5 | NO influences the D-aspartate evoked Ca^{2+}/Na$^+$ dynamics in cultured WT and nNOS$^{-/-}$ BG

The function of GLAST is tightly coupled to the sodium-calcium exchanger (NCX) reverse-mode activity (Kirischuk et al., 2007), and thus cytosolic changes in the concentrations of Ca^{2+} and Na$^+$ in BGs are indicators of overall NCX-GLAST functionality. We performed

live-cell imaging on WT and nNOS$^{-/-}$ cerebellar astrocytes to measure simultaneous changes of Na$^+$ and Ca^{2+} fluorescence in response to application of 100 μM D-aspartate, a compound that is known to activate GLAST (Balderas et al., 2014).

WT BG were left untreated (CON) or treated with either 50 nM 7N, 10 μM PKG$_i$, 1 μM UCPH, or 1 μM NCX$_i$. Application of D-aspartate to CON WT cells evoked an influx of Ca^{2+} relative to Na$^+$ that peaked within the first minute after D-aspartate application, and this ratio of Ca^{2+}/Na$^+$ remained elevated for the entire trace (Figure 9a–d). Notably, application of D-aspartate to WT cells pretreated with 7N significantly decreased the influx of Ca^{2+} relative to Na$^+$ when compared with WT CON trace (Figure 9a,e). Treating WT BG with PKG$_i$ showed a similar Ca^{2+}/Na$^+$ response to
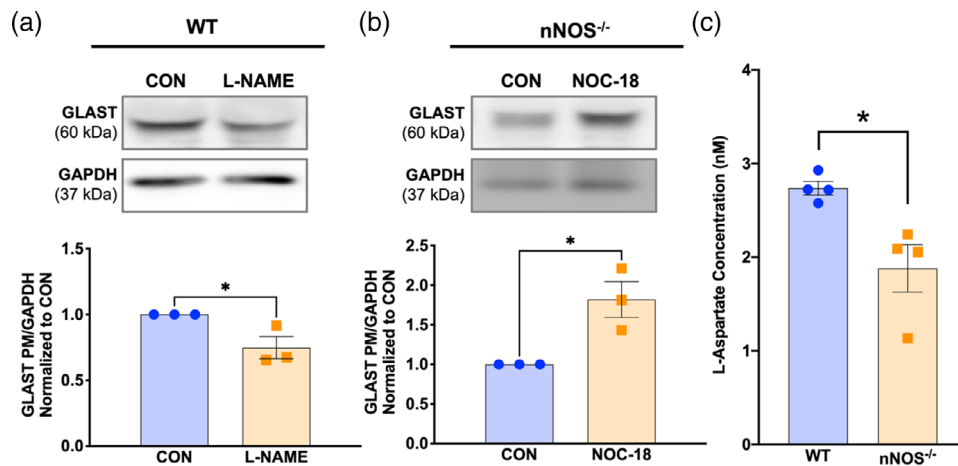
FIGURE 5 Nitric oxide modulates GLAST expression in an ex vivo model, and BG from nNOS$^{-/-}$ mice display deficits in GLAST functionality. (a) Representative western blot of total GLAST expression in WT slices that were left untreated (CON) or treated with 100 μM L-NAME. Bar graph represents $N = 3$ experimental replicates. $p = .0403$. (b) Representative western blot of total GLAST expression in nNOS$^{-/-}$ slices that were left untreated (CON) or treated with 300 μM NOC-18. Bar graph represents $N = 3$ experimental replicates. $p = .0222$. (c) Bar graph represents the concentration of L-aspartate taken up by WT and nNOS$^{-/-}$ astrocyte cultures after 30 min of L-aspartate treatment. $N = 4$ experimental replicates. $p = .0172$
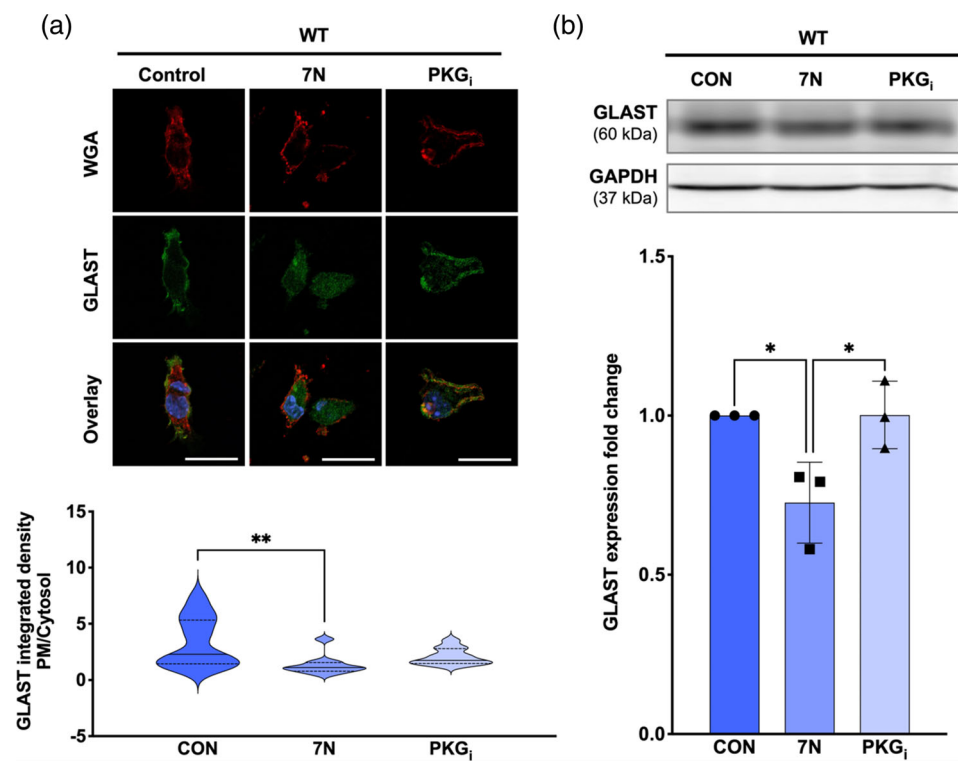

FIGURE 6 PM localization and total expression of GLAST is decreased in WT BG that were treated with a nNOS inhibitor. (a) Representative confocal images of WGA (red), GLAST (green), and nuclear staining DAPI (blue) fluorescence in WT BG that were untreated (CON) or treated with either 50 nM 7N or 10 μM PKG$_i$. Scale bar represents 50 μm. Violin plots represent the ratio of PM-localized GLAST immunofluorescence to cytosol-localized GLAST immunofluorescence. $N = 4$ experimental replicates per group; CON $n = 18$ cells, 7N $n = 10$ cells, PKG$_i$ $n = 11$ cells. $F_{(2, 36)} = 5.532$; $p = .0080$. (b) Representative western blot of GLAST expression in WT astrocyte cultures that were untreated (CON) or treated with 7N or PKG$_i$. Bar graph represents GLAST expression normalized to the housekeeping protein GAPDH. $N = 3$ biological replicates per group. $F_{(2, 6)} = 8.282$; $p = .0188$

D-aspartate as the WT CON BG (Figure 9b), while pretreatment with UCPH (Figure 8c) or NCX$_i$ (Figure 9d) significantly decreased the influx of Ca^{2+} relative to Na$^+$ when compared with the WT CON trace (Figure 9e). These results confirm that endogenous nNOS activity in cerebellar BG regulates NCX-coupled GLAST activity.
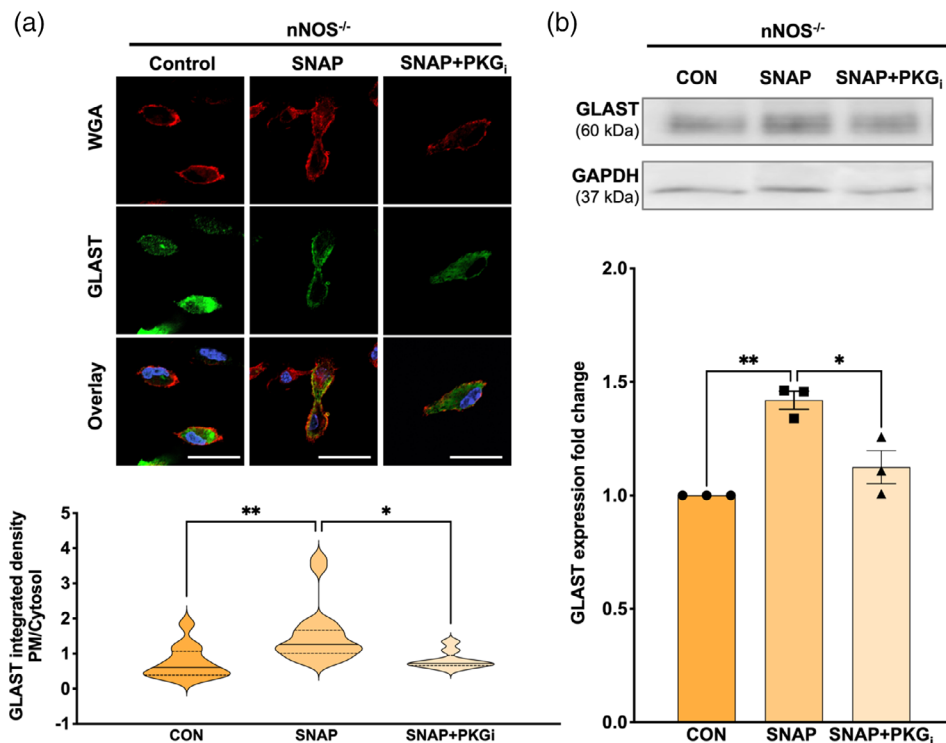
FIGURE 7 PM localization and total expression of GLAST is increased by NO application in nNOS$^{-/-}$ BG. (a) Representative confocal images of WGA (red), GLAST (green), and nuclear staining DAPI (blue) fluorescence in nNOS$^{-/-}$ BG that were left untreated (CON) or treated with either 250 µM SNAP or a combination of SNAP and 10 mM PKG$_i$ (SNAP+PKG$_i$). Scale bar represents 50 µm. Violin plots represent a ratio of PM-localized GLAST immunofluorescence to cytosol-localized GLAST immunofluorescence. $N = 4$ experimental replicates per group; CON $n = 12$ cells, SNAP $n = 19$ cells, SNAP+PKG$_i$ $n = 9$ cells. $F_{(2, 37)} = 7.022$; $p = .0026$. (b) Representative western blot of GLAST expression in nNOS$^{-/-}$ astrocyte cultures left untreated (CON) or treated with SNAP or SNAP+PKG$_i$. Bar graph represents GLAST expression normalized to the housekeeping protein GAPDH. $N = 3$ biological replicates per group. $F_{(2, 6)} = 20.24$; $p = .0022$
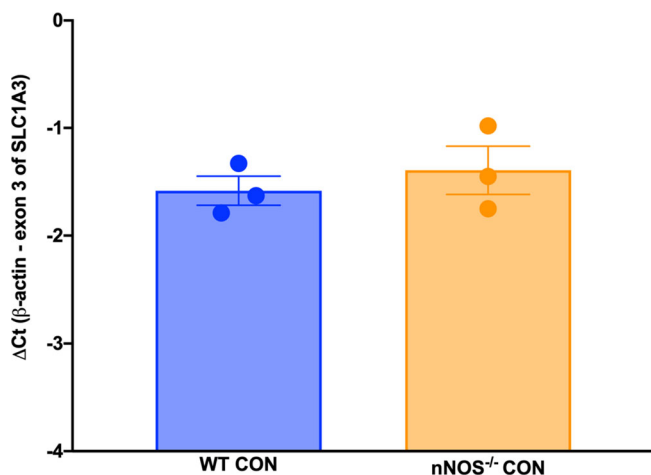

FIGURE 8 NO does not affect transcription of SLC1A3. The mRNA levels of SLC1A3, the gene encoding GLAST, were subtracted from mRNA levels of β-actin and presented graphically as ΔCt for WT and nNOS$^{-/-}$ primary cerebellar astrocyte cultures. No significant differences were noted between basal WT and nNOS$^{-/-}$ transcription $p = .5077$

As well, nNOS$^{-/-}$ BG were left untreated (CON), or were treated with either 250 µM SNAP, a combination of SNAP and PKG$_i$ (SNAP+PKG$_i$), UCPH, or NCX$_i$. Application of D-aspartate to CON

nNOS$^{-/-}$ BG evoked an influx of Ca^{2+} relative to Na$^+$ within the first 2 min after D-aspartate application, and this ratio of Ca^{2+}/Na$^+$ dropped to baseline levels after 2 min before slowly increasing for the remainder of the trace (Figure 10a). Importantly, pretreatment with SNAP evoked a significantly larger Ca^{2+}/Na$^+$ influx in response to D-aspartate when compared with CON nNOS$^{-/-}$ BG (Figure 10a). As well, pretreatment of SNAP+PKG$_i$ on nNOS$^{-/-}$ BG evoked a Ca^{2+}/Na$^+$ response similar to CON nNOS$^{-/-}$ BG, abolishing the observed effect from SNAP treatment alone (Figure 10b,e). In response to D-aspartate, both UCPH (Figure 10c) and NCX$_i$ (Figure 10d) pretreatment showed similar Ca^{2+}/Na$^+$ kinetics as CON nNOS$^{-/-}$ BG, which was significantly smaller than nNOS$^{-/-}$ BG in the presence of SNAP (Figure 10e). These results confirm NO can recover NCX-coupled GLAST activity in nNOS$^{-/-}$ BG.

4 | DISCUSSION

In the cerebellum, the relatively high concentration of nNOS-derived NO is crucial for the development of PN dendritic arborization and PN calcium homeostasis (Tellios et al., 2020). Although some evidence suggests that NO regulates GLAST function in the cerebellum (Balderas et al., 2014; Tiburcio-Félix et al., 2019), this study is the first to thoroughly characterize the role of nNOS/NO signaling on the regulation of
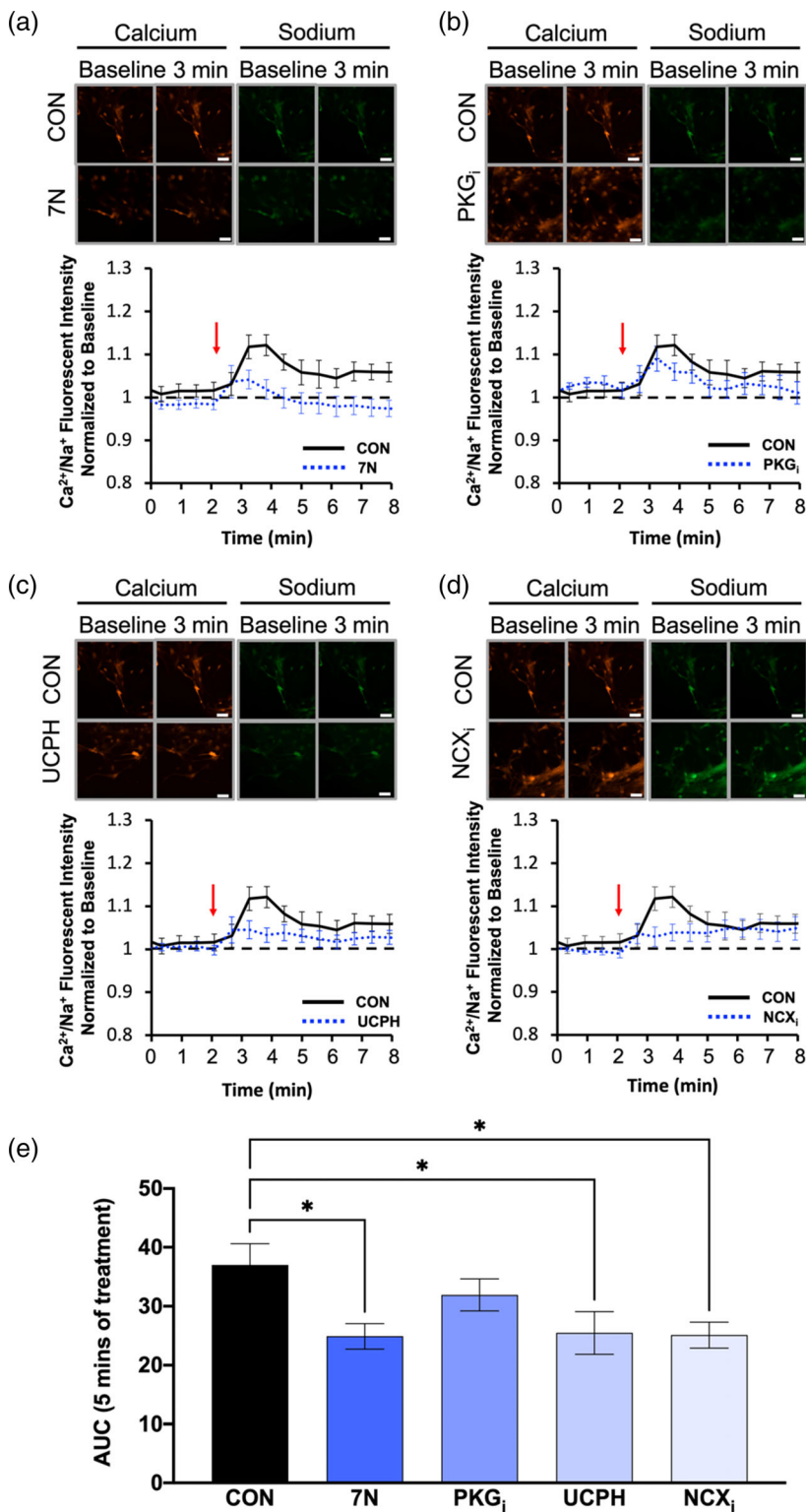
FIGURE 9 Ca^{2+}/Na^+ influx is downregulated by nNOS blockade in WT BG. (a–d) images from a–d represent calcium (red) and sodium (green) responses at baseline and 3 min after D-aspartate application (scale bar represents 100 μm). The representative time course of Ca^{2+}/Na^+ influx in response to application of D-aspartate, denoted by the red arrow. The black line represents the Ca^{2+}/Na^+ influx of WT BGs without a pretreatment (CON), while the blue line represents either WT BGs pretreated with 7N (a), PKG_i (b), UCPH (c), or NCX_i (d). Black, dashed line represents baseline Ca^{2+}/Na^+ conductance. (e) Bar graph represents the area under the curve (AUC) for each pretreatment visualized in a–d after 5 min of D-aspartate treatment. $N = 3$ experimental replicates. CON $n = 25$ cells, 7N $n = 24$ cells, PKG_i $n = 24$ cells, UCPH $n = 27$ cells, NCX_i $n = 21$ cells. $F(4, 130) = 3.408; p = .0110$

GLAST expression, localization, and functionality of cerebellar BGs using WT and nNOS$^{-/-}$ mice. Specifically, this study is the first to report two novel findings. First, BG morphology and GLAST expression across early murine postnatal stages are regulated by nNOS signaling. Second, the plasma membrane localization and trafficking of GLAST is regulated by NO, which facilitates GLAST coupling to the reverse mode NCX activity to mobilize calcium and sodium ions in BG.

4.1 | Morphological abnormalities are present in BG of young nNOS$^{-/-}$ mice

It has previously been reported that BG serve as important mediators of both granule cell differentiation and migration from the EGL to the IGL, as well as PN dendritic and synaptic growth from the PN layer to the pial surface (Altman, 1972; Ango et al., 2008; Lordkipanidze &

FIGURE 10 Ca^{2+}/Na$^+$ influx is downregulated by NO application in nNOS$^{-/-}$ BG. (a–d) Images from a–d represent calcium (red) and sodium (green) responses at baseline and 3 min after D-aspartate application (scale bar represents 100 μm). The representative time course of Ca^{2+}/Na$^+$ influx in response to application of D-aspartate, denoted by the red arrow. The black line represents the Ca^{2+}/Na$^+$ influx of nNOS$^{-/-}$ BGs without a pretreatment (CON), while the orange line represents either nNOS$^{-/-}$ BGs pre-treated with SNAP (a), SNAP +PKG$_i$ (b), UCPH (c), or NCX$_i$ (d). Black, dashed line represents baseline Ca^{2+}/Na$^+$ conductance. (e) Bar graph represents the area under the curve (AUC) for each pretreatment visualized in a–d after 5 min of D-aspartate treatment. N = 3 experimental replicates. CON n = 23 cells, SNAP n = 20 cells, SNAP+PKG$_i$ n = 26 cells, UCPH n = 25 cells, NCX$_i$ n = 25 cells. $F_{(4, 130)} = 4.723$; $p = .0014$
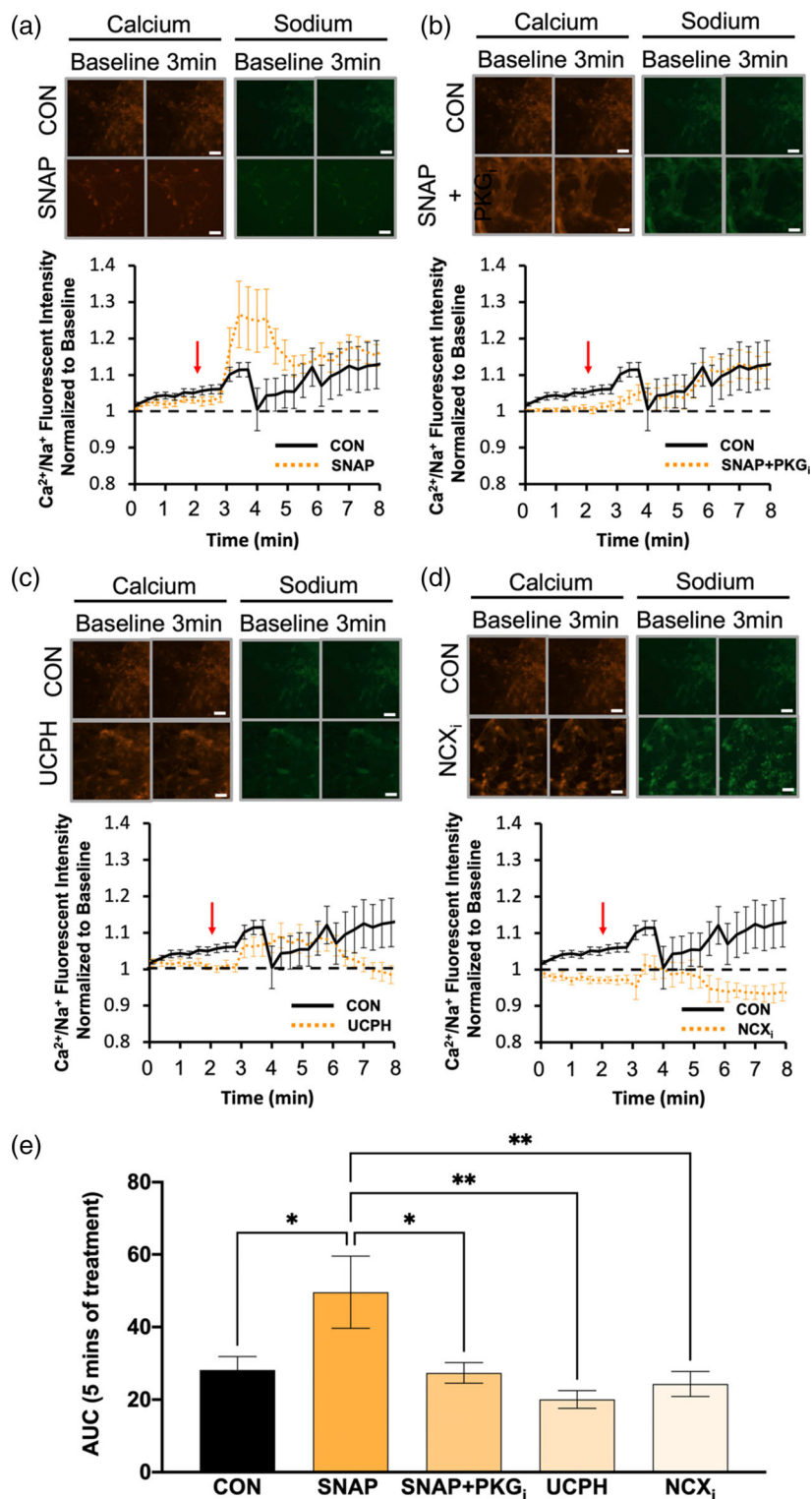
Dunaevsky, 2005; Xu et al., 2013). During early postnatal development (PD0–PD10), BG morphology transitions from distinct smooth lamellar processes that radiate toward the pial surface, to rough radial processes that contain outgrowths that work to ensheath PN synaptic connections with PFs and stellate cells (Lippman et al., 2008; Yamada et al., 2000). In the present study, our group discovered abnormally thick lamellar processes in nNOS$^{-/-}$ cerebella during PD3 and PD7

when compared with WT. An earlier study that explored BG morphology in the *weaver* cerebellar mutant mouse reported a similar BG morphology with abnormally thick lamellar processes, which this group denoted was the cause of PN and granule cell degeneration that presented later in life (Bignami & Dahl, 1974). Similarly, we have found stark PN dendritic deficits in the nNOS$^{-/-}$ mouse, specifically at PD7 (Tellios et al., 2020). This finding, when taken into consideration with

the BG morphological changes noted in this study, is not surprising as BG lamellar processes work to guide and promote PN dendritic growth toward the pial surface (Lordkipanidze & Dunaevsky, 2005).

BG lamellar processes guide the direction of PN dendritic growth by interacting closely with the tips of dendritic branches. Moreover, BG are able to influence PN dendritic growth and PN firing through a mechanism involving GLAST activity (Miyazaki et al., 2017; Perkins et al., 2018). In the present study, we observed a notable decrease in GLAST colocalization with CalB in nNOS$^{-/-}$ cerebella compared with WT. This finding implies a reduced ensheathment of PN dendritic spines and synapses by BG. As BG lamellar processes mature, radial outgrowths wrap around PN dendritic spines and protect synapses from excitotoxic damage (Lippman et al., 2008; Yamada et al., 2000). We previously showed that in adult nNOS$^{-/-}$ mice, there was an overall decrease in PN spine number compared with WT, and the majority of PN dendritic spines take the form of thin-type spines, as opposed to the predominant mushroom-type spine found on WT PNs (Tellios et al., 2020). Therefore, the PN deficits reported in nNOS$^{-/-}$ mice may be the result of aberrant BG growth, which is supported by multiple studies that report BG-specific deficits lead to the degeneration and loss of PNs (Takatsuru et al., 2006; Wang et al., 2011). Likewise, it is known that nNOS is expressed in supporting cells such as BGs, and not PNs (Ihara et al., 2006; Kugler & Drenckhahn, 1996; Tiburcio-Félix et al., 2019); therefore, it is possible that the structural and functional deficits of PNs in the nNOS$^{-/-}$ mice are at least partially the result of aberrant BG growth.

4.2 | GLAST protein expression is decreased in the cerebella of nNOS$^{-/-}$ mice

The morphological changes observed in nNOS$^{-/-}$ BG are associated with a decrease in GLAST plasma membrane protein expression in the cerebella of nNOS$^{-/-}$ mice across all time points in this study. Being the predominant transporter on BG, GLAST plays a crucial role in protecting PN synapses from excitotoxic damage. Although it has previously been reported that nNOS expression is upregulated in cultured BG following exposure to glutamate (Tiburcio-Félix et al., 2019) and that nNOS-derived NO signaling enhances glutamate uptake in BG (Balderas et al., 2014), our study is the first to report decreased GLAST expression from a lack of nNOS-derived NO production in vivo. Specifically, our assays revealed a decreased expression of GLAST protein in nNOS$^{-/-}$ cerebella across all postnatal time points when compared with WT cerebella. In addition, inhibition of the enzymatic activity of NOS in ex vivo WT cerebellar slices by LNAME or in cultured WT BG by 7N, significantly reduced GLAST expression. It is known that GLAST is an important modulator of synaptic function in the cerebellum, as it is crucial in regulating glutamate levels within the synaptic cleft. As well, decreased GLAST expression on astrocytes is a major factor that propagates a host of neurological disorders involving excitotoxic damage, including but not limited to, episodic ataxia, Alzheimer's disease, and retinal degeneration (Jen et al., 2005; Yanagisawa et al., 2020; Zoia et al., 2004). Decreased GLAST

expression has been related not only to PN morphological deficits, but deficits in spontaneous PN firing and spike activity (Perkins et al., 2018; Takatsuru et al., 2006). GLAST downregulation can happen for various reasons, including genetic causes such as expression of polynucleotide expansion of ataxin-7 as seen in spinocerebellar ataxia 7 (Custer et al., 2006), or as a result of external factors such as high concentrations of extracellular glutamate (Lopez-Bayghen & Ortega, 2004).

Importantly, our study also found that exogenous supplementation of NO significantly increased GLAST expression in ex vivo nNOS$^{-/-}$ cerebellar slices and in cultured nNOS$^{-/-}$ BG. This is in line with our previous report that discovered more PN branching in nNOS$^{-/-}$ cerebellar slices treated with NOC-18 (Tellios et al., 2020). As well, a crucial study has noted that decreased GLAST expression may be a result of overactive group 1 mGluRs (Gegelashvili et al., 2000). Interestingly, the nNOS$^{-/-}$ mouse itself may be a model of mGluR1 excitotoxicity, as this mouse line exhibits high levels of calcium-dependent protease activity, similar to levels experienced with WT slices treated with group 1 mGluR agonist, DHPG (Tellios et al., 2020).

4.3 | NO affects intracellular L-aspartate concentrations and upregulates GLAST expression on the plasma membrane of BG through a trafficking mechanism involving PKG

We next examined intracellular L-aspartate concentrations in cultured WT and nNOS$^{-/-}$ BG. After treatment with L-aspartate, our study noted lower cytosolic concentrations of L-aspartate in nNOS$^{-/-}$ BGs compared with WT BG, which can be associated with the lower level of GLAST protein expression that was observed in nNOS$^{-/-}$ BG when compared with WT BG. Importantly, Balderas et al., noted higher levels of D-aspartate uptake in cerebellar BG treated with NO-donor sodium nitroprusside as well as with treatment of cGMP analogue, dbcGMP (Balderas et al., 2014). The study by Balderas et al., highlighted the importance of the NO-cGMP-PKG pathway in upregulating GLAST activity in vitro. However, intracellular levels of L-aspartate alone are not indicative of GLAST function, as L-aspartate uptake and concentrations within BG can be affected by other metabolic processes within cells (Bender et al., 1997).

We further examined if GLAST localization in cultured WT and nNOS$^{-/-}$ BG was regulated by NO-PKG signaling. Notably, our assays detected a decrease in GLAST fluorescence on the plasma membrane of WT BG that were treated with nNOS inhibitor when compared with control WT BG. Importantly, treatment with PKG$_i$ on WT BG did not elicit any significant changes in GLAST localization when compared with control WT BG. Although many studies have reported that the activation of PKG results in an upregulation of GLAST expression and functionality in WT BGs (Balderas et al., 2014; Cabrera-Pastor et al., 2019), our results demonstrated that inhibition of PKG activity does not result in the internalization of GLAST, which must therefore be regulated by an alternative mechanism.
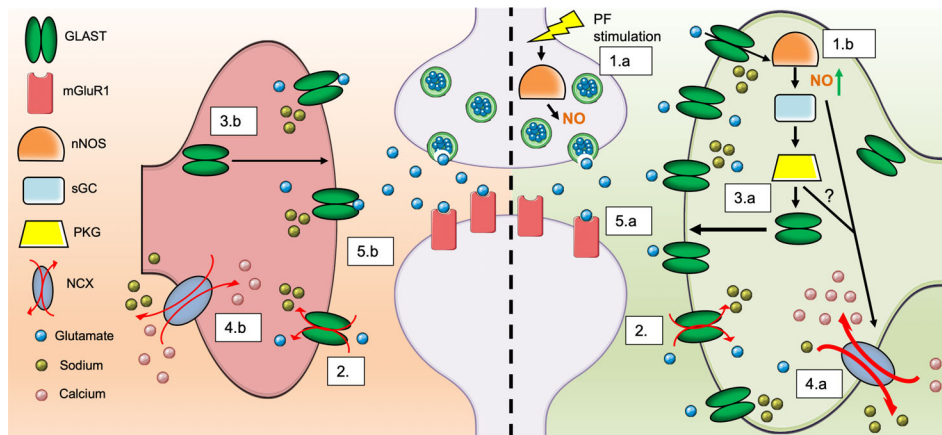
FIGURE 11 Schematic representation of GLAST regulation in relation to nNOS/NO signaling. The left side of the figure depicts a glutamatergic PN synapse in the absence of nNOS-derived NO signaling, while the right side depicts a physiological glutamatergic synapse with nNOS expression and NO production. (1.a) PF stimulation triggers the production of NO via calcium-dependent nNOS. (1.b) NO production can also be stimulated by glutamate uptake within BG, again through a calcium-dependent mechanism. (2) Glutamate released by PFs/CFs are uptake by GLAST and co-transported with 3 Na^+ ions into the BG cytosol. *Right side*: (3.a) NO produced by both PF terminals and BG will activate PKG through the classical NO-cGMP-PKG pathway, causing transport of GLAST to the BG PM. (4.a) Additionally, the increased Na^+ influx through GLAST activity, along with the presence of NO, causes a reversal of the NCX, allowing for Na^+ to be shuttled outside of the BG and causing an influx of Ca^{2+} into the BG. (5.a) As a result, appropriate glutamate clearance from the synaptic cleft occurs, contributing to the normal function of PNs in the cerebellum. *Left side*: (3.b) In the absence of nNOS/NO signaling, there is less activation of PKG and therefore less transport of GLAST to the BG PM. (4.b) Additionally, the lack of NO and lower Na^+ from active GLAST transporters results in lower activity of the NCX in reverse mode and less Ca^{2+} influx into the BG cytosol, which can cause BG process retraction and less BG ensheathment of the synaptic cleft. (5.b) As a result, the decrease in glutamate uptake efficiency will result in an overload of glutamate in the synaptic cleft, leading to PN excitotoxicity

Alternatively, an NO-donor increased GLAST fluorescence at the plasma membrane in nNOS$^{-/-}$ BG when compared with control nNOS$^{-/-}$ BG. Indeed, inhibiting PKG activity abolished the increased plasma membrane localization of GLAST observed from NO-donor treatment. In this case, it is apparent that NO signals through PKG to facilitate GLAST trafficking to the plasma membrane.

It is also important to consider that GLAST transcription remained unaffected between WT and nNOS$^{-/-}$ primary cells. In general, NO can act as a regulator of a variety of transcription factors, either by *S*-nitrosylation or through the classical NO-cGMP-PKG pathway (Pilz & Casteel, 2003; Sha & Marshall, 2012), although a previous study has documented that GLAST transcription is mediated by cAMP, pituitary adenylate cyclase-activating polypeptide, epidermal growth factor, and transforming growth factor α (Unger et al., 2012). However, recent studies have noted the presence of a variety of splice variants associated with GLAST expression, including GLAST 1a (skipping exon 3), GLAST 1b (skipping exon 9), and GLAST 1c (skipping exons 5 and 6) (Lee et al., 2012; Macnab et al., 2006; Macnab & Pow, 2007). Although this study specifically assayed for the transcriptional levels of exon 3, future studies may benefit from categorizing the expression levels of each of these splice variants within the nNOS$^{-/-}$ mouse model. Taken together, the data presented in this study indicate that NO facilitates GLAST localization to the plasma membrane of BGs through a trafficking mechanism involving activation of the PKG pathway.

4.4 | NO regulates the function of GLAST coupled to the NCX activity in the reverse mode

GLAST is a cotransporter utilizing the concentration gradient of Na^+ to bring glutamate into the cell. Importantly, GLAST activity is balanced by NCX activity, which transports 3 Na^+ in the opposite direction of 1 Ca^{2+} (Bauer et al., 2012). In resting astrocytes, 3 Na^+ are shuttled into the cell while 1 Ca^{2+} is transported to the extracellular space by NCX activity in the forward mode. However, when GLAST is activated in the presence of glutamate, L-aspartate, or D-aspartate, the NCX functions in the reverse mode to combat the sudden Na^+ influx from GLAST by ejecting Na^+ to the extracellular space and mobilizing Ca^{2+} into the cell (Kirischuk et al., 1997; Rojas et al., 2007). Considering this coupling action of GLAST and NCX, we utilized dual calcium and sodium fluorescent imaging to examine ion mobilization from NCX in response to D-aspartate activation of GLAST in cultures of WT and nNOS$^{-/-}$ BG.

Our assays revealed that control WT traces resulted in peak Ca^{2+} entry and Na^+ efflux within the first minute after application of D-aspartate, which was followed by a smaller, sustained increase in Ca^{2+}/Na^+ influx above baseline. Application of either UCPH or NCX$_i$ eliminated the peak influx of Ca^{2+}/Na^+ in response to D-aspartate and confirmed previous reports suspecting glutamate transporters such as GLAST are coupled to NCX activity, which may be required for GLAST activity in BG (Ibáñez et al., 2019; Kirischuk et al., 1997; Piccirillo et al., 2020).

Notably, inhibiting endogenous nNOS activity in WT BG resulted in a significant decrease in the Ca^{2+}/Na^+ ratio when compared with control WT BG, while supplementing NO to the $nNOS^{-/-}$ BG significantly elevated the Ca^{2+}/Na^+ influx when compared with control $nNOS^{-/-}$ BG, confirming that NO critically controls the coupled activity of GLAST and NCX. Interestingly, treating WT BG with PKG_i did not affect the Ca^{2+}/Na^+ ratio in response D-aspartate when compared with WT controls, while treating $nNOS^{-/-}$ BG with PKG_i significantly abolished the Ca^{2+}/Na^+ ratio observed from $nNOS^{-/-}$ BG that had NO supplemented in their culture conditions. These trends noted from live-cell imaging of calcium and sodium fluorescence in response to D-aspartate are substantiated by the fluorescent localization of GLAST protein on the plasma membrane in WT and $nNOS^{-/-}$ BG cultures. PKG inhibition on WT BG displayed no change in either plasma membrane localization of GLAST or Ca^{2+}/Na^+ ratio when compared with WT control BG while PKG inhibition on $nNOS^{-/-}$ BG that had NO supplemented in their culture conditions displayed both reduced plasma membrane localization of GLAST as well as reduced Ca^{2+}/Na^+ ratio when compared with $nNOS^{-/-}$ BG that had NO supplemented in their culture conditions. These data further demonstrate that NO signaling regulates the function of GLAST coupled to NCX activity in the reverse mode, possibly through GLAST trafficking to the plasma membrane in a PKG dependent mechanism. Further analysis of the coupling between GLAST and the NCX in relation to NO signaling would provide insight into novel therapeutic options for glutamate transporter dysfunction.

In general, Ca^{2+} influx is critical for BG to maintain appropriate physiological growth and functionality. Specialized Ca^{2+}-permeable AMPA receptors are found on BG and are stimulated by glutamate but not by L- or D-aspartate (Lopez-Bayghen & Ortega, 2004; Metea & Newman, 2006). A previous study noted that viral delivery of the GluR2 gene into BG caused their Ca^{2+}-permeable AMPA receptors to become Ca^{2+}-impermeable, which resulted in retraction of BG processes and less PN ensheathment (Iino et al., 2001), similar to what we observed in $nNOS^{-/-}$ BG. Furthermore, overexpression of Ca^{2+}-permeable receptors on BG resulted in BG process growth and extension (Ishiuchi et al., 2007). Therefore, the reduced Ca^{2+} influx and aberrant phenotype that we noted in $nNOS^{-/-}$ BG aligns well with previous findings that reports Ca^{2+} signaling is important for the function and activity of BG.

In summary, results from this study demonstrate a novel role for nNOS-derived NO signaling in regulating BG morphological development, GLAST expression, and GLAST functionality. As depicted in Figure 11, we propose that under physiological conditions, BG express GLAST to remove excessive glutamate that is released from PFs. During this process, NO derived from nNOS located in PFs and BG leads to an upregulation of GLAST expression and functionality through NO-cGMP-PKG pathway. As well, NO influences the activity of GLAST coupled to the NCX channel working in the reverse mode to shuttle calcium into BG, which is a common indicator of GLAST function (Nashida et al., 2011). Under the regulation of NO, BG ensheath PN synapses whereby expression of GLAST can remove excess glutamate from the synaptic cleft to combat excitotoxicity on PN during development. However, a lack of nNOS-derived NO, results in less BG ensheathment of PNs, less GLAST expression, less glutamate uptake, and more mGluR1 stimulation on PNs that leads to excitotoxicity during development (Tellios et al., 2020). Further analysis of the coupling between GLAST and the NCX in relation to NO would provide insight into novel therapeutic options for glutamate transporter dysfunction.

CONFLICT OF INTEREST

The authors declare no competing financial or non-financial interests.

DATA AVAILABILITY STATEMENT

The data that support the findings of this study are available from the corresponding author upon reasonable request.

ORCID

Vasiliki Tellios https://orcid.org/0000-0002-2976-9951
Matthew J. E. Maksoud https://orcid.org/0000-0003-1265-2797

REFERENCES

Altman, J. (1972). Postnatal development of the cerebellar cortex in the rat. I. The external germinal layer and the transitional molecular layer. *The Journal of Comparative Neurology, 145*(3), 353–397. https://doi.org/10.1002/cne.901450305

Ango, F., Wu, C., Van Der Want, J. J., Wu, P., Schachner, M., & Huang, Z. J. (2008). Bergmann glia and the recognition molecule CHL1 organize GABAergic axons and direct innervation of Purkinje cell dendrites. *PLoS Biology, 6*(4), 739–756. https://doi.org/10.1371/journal.pbio.0060103

Balderas, A., Guillem, A. M., Martínez-Lozada, Z., Hernández-Kelly, L. C., Aguilera, J., & Ortega, A. (2014). GLAST/EAAT1 regulation in cultured Bergmann glia cells: Role of the NO/cGMP signaling pathway. *Neurochemistry International, 73*(1), 139–145. https://doi.org/10.1016/j.neuint.2013.10.011

Bauer, D. E., Jackson, J. G., Genda, E. N., Montoya, M. M., Yudkoff, M., & Robinson, M. B. (2012). The glutamate transporter, GLAST, participates in a macromolecular complex that supports glutamate metabolism. *Neurochemistry International, 61*(4), 566–574. https://doi.org/10.1016/j.neuint.2012.01.013

Bender, A. S., Woodbury, D. M., White, H. S. (1997). The rapid L- and D-aspartate uptake in cultured astrocytes. *Neurochemical Research, 22*(6), 721–726. https://doi.org/10.1023/a:1027358211472

Bignami, A., & Dahl, D. (1974). The development of Bergmann glia in mutant mice with cerebellar malformations: Reeler, staggerer and weaver. Immunofluorescence study with antibodies to the glial fibrillary acidic protein. *The Journal of Comparative Neurology, 155*(2), 219–229. https://doi.org/10.1002/cne.901550207

Bredt, D. S., Hwang, P. M., & Snyder, S. H. (1990). Localization of nitric oxide synthase indicating a neural role for nitric oxide. *Nature, 347*(6295), 768–770. https://doi.org/10.1038/347768a0

Bredt, D. S., & Snyder, S. H. (1989). Nitric oxide mediates glutamate-linked enhancement of cGMP levels in the cerebellum (N-methyl-D-aspartate/arginine/citrulline/climbing fibers/inositol phospholipid cycle). *Neurobiology, 86*, 9030–9033.

Brown, S. P., Brenowitz, S. D., & Regehr, W. G. (2003). Brief presynaptic bursts evoke synapse-specific retrograde inhibition mediated by endogenous cannabinoids. *Nature Neuroscience*, 6(10), 1048–1057. https://doi.org/10.1038/nn1126

Cabrera-Pastor, A., Arenas, Y. M., Taoro-Gonzalez, L., Montoliu, C., & Felipo, V. (2019). Chronic hyperammonemia alters extracellular glutamate, glutamine and GABA and membrane expression of their transporters in rat cerebellum. Modulation by extracellular cGMP. *Neuropharmacology*, 161, 107496. https://doi.org/10.1016/j.neuropharm.2019.01.011

Campese, V. M., Sindhu, R. K., Ye, S., Bai, Y., Vaziri, N. D., & Jabbari, B. (2006). Regional expression of NO synthase, NAD (P) H oxidase and superoxide dismutase in the rat brain. *Brain Research*, 1134, 27–32. https://doi.org/10.1016/j.brainres.2006.11.067

Contestabile, A. (2012). Role of nitric oxide in cerebellar development and function: Focus on granule neurons. *Cerebellum*, 11(1), 50–61. https://doi.org/10.1007/s12311-010-0234-1

Custer, S. K., Garden, G. A., Gill, N., Rueb, U., Libby, R. T., Schultz, C., Guyenet, S. J., Deller, T., Westrum, L. E., Sopher, B. L., & la Spada, A. R. (2006). Bergmann glia expression of polyglutamine-expanded ataxin-7 produces neurodegeneration by impairing glutamate transport. *Nature Neuroscience*, 9(10), 1302–1311. https://doi.org/10.1038/nn1750

Daniel, H., Levenes, C., & Crépel, F. (1998). Cellular mechanisms of cerebellar LTD. *Trends in Neurosciences*, 21(9), 401–407. https://doi.org/10.1016/S0166-2236(98)01304-6

Gegelashvili, G., Dehnes, Y., Danbolt, N. C., & Schousboe, A. (2000). The high-affinity glutamate transporters GLT1, GLAST, and EAAT4 are regulated via different signalling mechanisms. *Neurochemistry International*, 37(2–3), 163–170. https://doi.org/10.1016/S0197-0186(00)00019-X

Huang, P. L., Dawson, T. M., Bredt, D. S., Snyder, S. H., & Fishman, M. C. (1993). Targeted disruption of the neuronal nitric oxide synthase gene. *Cell*, 75(7), 1273–1286. https://doi.org/10.1016/0092-8674(93)90615-w

Ibáñez, I., Bartolomé-Martín, D., Piniella, D., Giménez, C., & Zafra, F. (2019). Activity dependent internalization of the glutamate transporter GLT-1 requires calcium entry through the NCX sodium/calcium exchanger. *Neurochemistry International*, 123, 125–132. https://doi.org/10.1016/j.neuint.2018.03.012

Ihara, H., Kuwamura, M., Atsuta, M., Nihonmatsu, I., Okada, T., Mukamoto, M., & Kozaki, S. (2006). Expression of neuronal nitric oxide synthase variant, nNOS-μ, in rat brain. *Nitric Oxide: Biology and Chemistry*, 15(1), 13–19. https://doi.org/10.1016/j.niox.2005.11.011

Iino, M., Goto, K., Kakegawa, W., Okado, H., Sudo, M., Ishiuchi, S., Miwa, A., Takayasu, Y., Saito, I., Tsuzuki, K., & Ozawa, S. (2001). Glia-synapse interaction through Ca2+-permeable AMPA receptors in Bergmann glia. *Science*, 292(5518), 926–929. https://doi.org/10.1126/science.1058827

Ishiuchi, S., Yoshida, Y., Sugawara, K., Aihara, M., Ohtani, T., Watanabe, T., Saito, N., Tsuzuki, K., Okado, H., Miwa, A., Nakazato, Y., & Ozawa, S. (2007). Ca2+-permeable AMPA receptors regulate growth of human glioblastoma via Akt activation. *Journal of Neuroscience*, 27(30), 7987–8001. https://doi.org/10.1523/JNEUROSCI.2180-07.2007

Jen, J. C., Wan, J., Palos, T. P., Howard, B. D., & Baloh, R. W. (2005). Mutation in the glutamate transporter EAAT1 causes episodic ataxia, hemiplegia, and seizures. *Neurology*, 65(4), 529–534. https://doi.org/10.1212/01.WNL.0000172638.58172.5a

Kirischuk, S., Kettenmann, H., & Verkhratsky, A. (1997). Na + /Ca 2+ exchanger modulates kainate-triggered Ca 2+ signaling in Bergmann glial cells in situ. *The FASEB Journal*, 11(7), 566–572. https://doi.org/10.1096/fasebj.11.7.9212080

Kirischuk, S., Kettenmann, H., & Verkhratsky, A. (2007). Membrane currents and cytoplasmic sodium transients generated by glutamate transport in Bergmann glial cells. *Pflügers Archiv - European Journal of Physiology*, 454(2), 245–252. https://doi.org/10.1007/s00424-007-0207-5

Koziol, L. F., Budding, D. E., & Chidekel, D. (2012). From movement to thought: Executive function, embodied cognition, and the cerebellum. *The Cerebellum*, 11(2), 505–525. https://doi.org/10.1007/s12311-011-0321-y

Kriegsfeld, L. J., Eliasson, M. J., Demas, G. E., Blackshaw, S., Dawson, T. M., Nelson, R. J., & Snyder, S. H. (1999). Nocturnal motor coordination deficits in neuronal nitric oxide synthase knock-out mice. *Neuroscience*, 89(2), 311–315.

Kugler, P., & Drenckhahn, D. (1996). Astrocytes and Bergmann glia as an important site of nitric oxide synthase I. *Glia*, 16, 165–173. https://doi.org/10.1002/(SICI)1098-1136(199602)16:2

Lee, A., Anderson, A. R., Beasley, S. J., Barnett, N. L., Poronnik, P., & Pow, D. V. (2012). A new splice variant of the glutamate–aspartate transporter: Cloning and immunolocalization of GLAST1c in rat, pig and human brains. *Journal of Chemical Neuroanatomy*, 43(1), 52–63. https://doi.org/10.1016/J.JCHEMNEU.2011.10.005

Lehre, K. P., & Danbolt, N. C. (1998). The number of glutamate transporter subtype molecules at glutamatergic synapses: Chemical and stereological quantification in young adult rat brain. *The Journal of Neuroscience*, 18(21), 8751–8757. https://doi.org/10.1523/JNEUROSCI.18-21-08751.1998

Liang, J., Chao, D., Sandhu, H. K., Yu, Y., Zhang, L., Balboni, G., Kim, D. H., & Xia, Y. (2014). δ-Opioid receptors up-regulate excitatory amino acid transporters in mouse astrocytes. *British Journal of Pharmacology*, 171(23), 5417–5430. https://doi.org/10.1111/bph.12857

Lippman, J. J., Lordkipanidze, T., Buell, M. E., Yoon, S. O., & Dunaevsky, A. (2008). Morphogenesis and regulation of Bergmann glial processes during Purkinje cell dendritic spine ensheathment and synaptogenesis. *Glia*, 56(13), 1463–1477. https://doi.org/10.1002/glia.20712

Lo, C. J., Leake, M. C., & Berry, R. M. (2006). Fluorescence measurement of intracellular sodium concentration in single Escherichia coli cells. *Biophysical Journal*, 90(1), 357–365. https://doi.org/10.1529/biophysj.105.071332

Lopez-Bayghen, E., & Ortega, A. (2004). Glutamate-dependent transcriptional regulation of GLAST: Role of PKC. *Journal of Neurochemistry*, 91(1), 200–209. https://doi.org/10.1111/j.1471-4159.2004.02706.x

Lordkipanidze, T., & Dunaevsky, A. (2005). Purkinje cell dendrites grow in alignment with Bergmann glia. *Glia*, 51(3), 229–234. https://doi.org/10.1002/glia.20200

Macnab, L. T., & Pow, D. V. (2007). Central nervous system expression of the exon 9 skipping form of the glutamate transporter GLAST. *Neuroreport*, 18(8), 741–745. https://doi.org/10.1097/WNR.0B013E3280C143B0

Macnab, L. T., Williams, S. M., & Pow, D. V. (2006). Expression of the exon 3 skipping form of GLAST, GLAST1a, in brain and retina. *Neuroreport*, 17(18), 1867–1870. https://doi.org/10.1097/WNR.0B013E328010B898

Maksoud, M. J. E., Tellios, V., An, D., Xiang, Y.-Y., & Lu, W.-Y. (2019). Nitric oxide upregulates microglia phagocytosis and increases transient receptor potential vanilloid type 2 channel expression on the plasma membrane. *Glia*, 67(12), 2294–2311. https://doi.org/10.1002/glia.23685

Maksoud, M. J. E., Tellios, V., Xiang, Y.-Y., & Lu, W.-Y. (2020). Nitric oxide signaling inhibits microglia proliferation by activation of protein kinase-G. *Nitric Oxide: Biology and Chemistry*, 94, 125–134. https://doi.org/10.1016/j.niox.2019.11.005

Manto, M., Bower, J. M., Conforto, A. B., Delgado-García, J. M., da Guarda, S. N. F., Gerwig, M., Habas, C., Hagura, N., Ivry, R. B., Mariën, P., Molinari, M., Naito, E., Nowak, D. A., Oulad Ben Taib, N., Pelisson, D., Tesche, C. D., Tilikete, C., & Timmann, D. (2012). Consensus paper: Roles of the cerebellum in motor control—The diversity of ideas on cerebellar involvement in movement. *The Cerebellum*, 11(2), 457–487. https://doi.org/10.1007/s12311-011-0331-9

Martínez-Lozada, Z., Hernández-Kelly, L. C., Aguilera, J., López-Bayghen, E., & Ortega, A. (2011). Signaling through EAAT-1/GLAST in

cultured Bergmann glia cells. *Neurochemistry International*, 59(6), 871–879. https://doi.org/10.1016/j.neuint.2011.07.015

Matsuda, T., Arakawa, N., Takuma, K., Kishida, Y., Kawasaki, Y., Sakaue, M., Takahashi, K., Takahashi, T., Suzuki, T., Ota, T., Hamano-Takahashi, A., Onishi, M., Tanaka, Y., Kameo, K., & Baba, A. (2001). SEA0400, a novel and selective inhibitor of the Na+-Ca2+ exchanger, attenuates reperfusion injury in the in vitro and in vivo cerebral ischemic models. *The Journal of Pharmacology and Experimental Therapeutics*, 298(1), 249–256.

Matyash, V., Filippov, V., Mohrhagen, K., & Kettenmann, H. (2001). Nitric oxide signals parallel fiber activity to Bergmann glial cells in the mouse cerebellar slice. *Molecular and Cellular Neuroscience*, 18(6), 664–670. https://doi.org/10.1006/mcne.2001.1047

Metea, M. R., & Newman, E. A. (2006). Calcium signaling in specialized glial cells. *Glia*, 54(7), 650–655. https://doi.org/10.1002/glia.20352

Miyazaki, T., Yamasaki, M., Hashimoto, K., Kohda, K., Yuzaki, M., Shimamoto, K., Tanaka, K., Kano, M., & Watanabe, M. (2017). Glutamate transporter GLAST controls synaptic wrapping by Bergmann glia and ensures proper wiring of Purkinje cells. *Proceedings of the National Academy of Sciences of the United States of America*, 114(28), 7438–7443. https://doi.org/10.1073/pnas.1617330114

Namiki, S., Kakizawa, S., Hirose, K., & Iino, M. (2005). NO signalling decodes frequency of neuronal activity and generates synapse-specific plasticity in mouse cerebellum. *The Journal of Physiology*, 566, 849–863. https://doi.org/10.1113/jphysiol.2005.088799

Nashida, T., Takuma, K., Fukuda, S., Kawasaki, T., Takahashi, T., Baba, A., Ago, Y., & Matsuda, T. (2011). The specific Na+/Ca2+ exchange inhibitor SEA0400 prevents nitric oxide-induced cytotoxicity in SH-SY5Y cells. *Neurochemistry International*, 59(1), 51–58. https://doi.org/10.1016/j.neuint.2011.03.026

Nelson, R., Demas, G., Huang, P., Fishman, M., Dawson, V., Dawson, T., & Snyder, S. (1995). Behavioural abnormalities in male mice lacking neuronal nitric oxide synthase. *Nature*, 378(6555), 383–386. https://doi.org/10.1038/378383a0

Perego, C., Vanoni, C., Bossi, M., Massari, S., Basudev, H., Longhi, R., & Pietrini, G. (2000). The GLT-1 and GLAST glutamate transporters are expressed on morphologically distinct astrocytes and regulated by neuronal activity in primary hippocampal cocultures. *Journal of Neurochemistry*, 75(3), 1076–1084. https://doi.org/10.1046/j.1471-4159.2000.0751076.x

Perkins, E. M., Clarkson, Y. L., Suminaite, D., Lyndon, A. R., Tanaka, K., Rothstein, J. D., Skehel, P. A., Wyllie, D. J. A., & Jackson, M. (2018). Loss of cerebellar glutamate transporters EAAT4 and GLAST differentially affects the spontaneous firing pattern and survival of Purkinje cells. *Human Molecular Genetics*, 27(15), 2614–2627. https://doi.org/10.1093/hmg/ddy169

Piccirillo, S., Magi, S., Castaldo, P., Preziuso, A., Lariccia, V., & Amoroso, S. (2020). NCX and EAAT transporters in ischemia: At the crossroad between glutamate metabolism and cell survival. *Cell Calcium*, 86, 102160. https://doi.org/10.1016/j.ceca.2020.102160

Pilz, R. B., & Casteel, D. E. (2003). Regulation of gene expression by cyclic GMP. *Circulation Research*, 93(11), 1034–1046. https://doi.org/10.1161/01.RES.0000103311.52853.48

Rojas, H., Colina, C., Ramos, M., Benaim, G., Jaffe, E. H., Caputo, C., & DiPolo, R. (2007). Na+ entry via glutamate transporter activates the reverse Na+/Ca2+ exchange and triggers Cai2+ -induced Ca2+ release in rat cerebellar Type-1 astrocytes. *Journal of Neurochemistry*, 100(5), 1188–1202. https://doi.org/10.1111/j.1471-4159.2006.04303.x

Rose, C. R., Ziemens, D., & Verkhratsky, A. (2020). On the special role of NCX in astrocytes: Translating Na+-transients into intracellular Ca2+ signals. *Cell Calcium*, 86, 102154. https://doi.org/10.1016/j.ceca.2019.102154

Sha, Y., & Marshall, H. E. (2012). S-nitrosylation in the regulation of gene transcription. *Biochimica et Biophysica Acta (BBA) - General Subjects*, 1820(6), 701–711. https://doi.org/10.1016/J.BBAGEN.2011.05.008

Takatsuru, Y., Takayasu, Y., Iino, M., Nikkuni, O., Ueda, Y., Tanaka, K., & Ozawa, S. (2006). Roles of glial glutamate transporters in shaping EPSCs at the climbing fiber-Purkinje cell synapses. *Neuroscience Research*, 54(2), 140–148. https://doi.org/10.1016/j.neures.2005.11.002

Tellios, V., Maksoud, M. J. E., Xiang, Y. Y., & Lu, W. Y. (2020). Nitric oxide critically regulates Purkinje neuron dendritic development through a metabotropic glutamate receptor type 1–mediated mechanism. *Cerebellum*, 19(4), 510–526. https://doi.org/10.1007/s12311-020-01125-7

Tiburcio-Félix, R., Cisneros, B., Hernández-Kelly, L. C. R., Hernández-Contreras, M. A., Luna-Herrera, J., Rea-Hernández, I., Jiménez-Aguilar, R., Olivares-Bañuelos, T. N., & Ortega, A. (2019). Neuronal nitric oxide synthase in cultured cerebellar Bergmann glia: Glutamate-dependent regulation. *ACS Chemical Neuroscience*, 10(6), 2668–2675. https://doi.org/10.1021/acschemneuro.8b00656

Unger, T., Lakowa, N., Bette, S., & Engele, J. (2012). Transcriptional regulation of the GLAST/EAAT-1 gene in rat and man. *Cellular and Molecular Neurobiology*, 32(4), 539–547. https://doi.org/10.1007/S10571-011-9790-2/FIGURES/2

Wang, D.-J., Su, L.-D., Wang, Y.-N., Yang, D., Sun, C.-L., Zhou, L., Wang, X. X., & Shen, Y. (2014). Long-term potentiation at cerebellar parallel fiber-Purkinje cell synapses requires presynaptic and postsynaptic signaling cascades. *Journal of Neuroscience*, 34(6), 2355–2364. https://doi.org/10.1523/JNEUROSCI.4064-13.2014

Wang, X., Imura, T., Sofroniew, M. V., & Fushiki, S. (2011). Loss of adenomatous polyposis coli in Bergmann glia disrupts their unique architecture and leads to cell nonautonomous neurodegeneration of cerebellar Purkinje neurons. *Glia*, 59(6), 857–868. https://doi.org/10.1002/glia.21154

Xu, H., Yang, Y., Tang, X., Zhao, M., Liang, F., Xu, P., Hou, B., Xing, Y., Bao, X., & Fan, X. (2013). Bergmann glia function in granule cell migration during cerebellum development. *Molecular Neurobiology*, 47(2), 833–844. https://doi.org/10.1007/s12035-013-8405-y

Yamada, K., Fukaya, M., Shibata, T., Kurihara, H., Tanaka, K., Inoue, Y., & Watanabe, M. (2000). Dynamic transformation of Bergmann glial fibers proceeds in correlation with dendritic outgrowth and synapse formation of cerebellar Purkinje cells. *The Journal of Comparative Neurology*, 418(1), 106–120. https://doi.org/10.1002/(SICI)1096-9861(20000228)418:1<106::AID-CNE8>3.0.CO;2-N

Yanagisawa, M., Namekata, K., Aida, T., Katou, S., Takeda, T., Harada, T., Fuse, N., the Glaucoma Gene Research Group, & Tanaka, K. (2020). EAAT1 variants associated with glaucoma. *Biochemical and Biophysical Research Communications*, 529(4), 943–949. https://doi.org/10.1016/j.bbrc.2020.06.099

Zoia, C., Cogliati, T., Tagliabue, E., Cavaletti, G., Sala, G., Galimberti, G., Rivolta, I., Rossi, V., Frattola, L., & Ferrarese, C. (2004). Glutamate transporters in platelets: EAAT1 decrease in aging and in Alzheimer's disease. *Neurobiology of Aging*, 25(2), 149–157. https://doi.org/10.1016/S0197-4580(03)00085-X

SUPPORTING INFORMATION

Additional supporting information may be found in the online version of the article at the publisher's website.